The Astrophysical Journal, 886:80 (23pp), 2019 December 1 https://doi.org/10.3847/1538-4357/ab4d4f

The Most Massive Galaxies with Large Depleted Cores: Structural Parameter Relations and Black Hole Masses

Bililign T. Dullo
Departamento de Física de la Tierra y Astrofísica, Instituto de Física de Partículas y del Cosmos IPARCOS, Universidad Complutense de Madrid, E-28040 Madrid, Spain; bdullo@ucm.es
Received 2019 August 12; revised 2019 September 17; accepted 2019 October 8; published 2019 November 22

Abstract

Luminous spheroids ($M_V \lesssim -21.50 \pm 0.75$ mag) contain partially depleted cores with sizes (R_b) typically 0.02–0.5 kpc. However, galaxies with $R_b > 0.5$ kpc are rare and poorly understood. Here, we perform detailed decompositions of the composite surface brightness profiles, extracted from archival *Hubble Space Telescope* and ground-based images, of 12 extremely luminous "large-core" galaxies that have $R_b > 0.5$ kpc and $M_V \lesssim -23.50 \pm 0.10$ mag, fitting a core-Sérsic model to the galaxy spheroids. Using 28 "normal-core" (i.e., $R_b < 0.5$ kpc) galaxies and one "large-core" (i.e., $R_b > 0.5$ kpc) galaxy from the literature, we constructed a final sample of 41 core-Sérsic galaxies. We find that large-core spheroids (with stellar masses $M_* \gtrsim 10^{12} M_\odot$) are not simple high-mass extensions of the less luminous normal-core spheroids having $M_* \sim 8 \times 10^{10}$–$10^{12} M_\odot$. While the two types follow the same strong relations between the spheroid luminosity L_V and R_b ($R_b \propto L_V^{1.38\pm0.13}$), and the spheroid half-light radius R_e ($R_e \propto L_V^{1.08\pm0.09}$, for ellipticals plus Brightest Cluster Galaxies), we discover a break in the core-Sérsic σ–L_V relation occurring at $M_V \sim -23.50 \pm 0.10$ mag. Furthermore, we find a strong log-linear R_b–M_{BH} relation for the 11 galaxies in the sample with directly determined supermassive black hole (SMBH) masses M_{BH}—3/11 galaxies are large-core galaxies—such that $R_b \propto M_{BH}^{0.83\pm0.10}$. However, for the large-core galaxies the SMBH masses estimated from the M_{BH}–σ and core-Sérsic M_{BH}–L relations are undermassive, by up to a factor of 40, relative to expectations from their large R_b values, confirming earlier results. Our findings suggest that large-core galaxies harbor overmassive SMBHs ($M_{BH} \gtrsim 10^{10} M_\odot$), considerably ($\sim$3.7–15.6$\sigma$ and $\sim$0.6–1.7σ) larger than expectations from the spheroid σ and L, respectively. We suggest that the R_b–M_{BH} relation can be used to estimate SMBH masses in the most massive galaxies.

Unified Astronomy Thesaurus concepts: Supermassive black holes (1663); cD galaxies (209); Elliptical galaxies (456); Lenticular galaxies (915); Galaxy photometry (611); Galaxy nuclei (609); Galaxy structure (622)

1. Introduction

It is now believed that all massive galaxies contain a supermassive black hole (SMBH) at their center (Magorrian et al. 1998; Richstone et al. 1998; Ferrarese & Ford 2005). The connection between SMBHs and the properties of their host galaxies has been a subject of ongoing interest (see Kormendy & Ho 2013; Graham 2016 for recent reviews). SMBH masses (M_{BH}) scale with a wide range of host galaxy properties such as the stellar velocity dispersion (σ; Ferrarese & Merritt 2000; Gebhardt et al. 2000) and bulge luminosity (L; Kormendy & Richstone 1995; Magorrian et al. 1998; Marconi & Hunt 2003). In addition, observations reveal partially depleted cores—a flattening in the inner stellar light distributions of galaxies—that are explained as an imprint left by binary SMBHs on the central structures of their host galaxies.

Luminous spheroids ($M_V \lesssim -21.50 \pm 0.75$ mag), for the most part, possess depleted cores. In the hierarchical structure formation model, the brightest and most massive galaxies are built through generations of galaxy merger events (e.g., Toomre & Toomre 1972; White & Rees 1978; Schweizer 1982; Barnes 1988; Kauffmann et al. 1993; De Lucia & Blaizot 2007; Laporte et al. 2013). SMBH binaries invariably form in such galaxy mergers (e.g., Komossa et al. 2003; Rodriguez et al. 2006; Bianchi et al. 2008; Burke-Spolaor 2011; Barrows et al. 2012; Comerford et al. 2015; Goulding et al. 2019). *N*-body simulations suggest that depleted cores are generated via three-body interactions between inner stars from the galaxy core regions and orbitally decaying SMBH binaries that form in major, "dry" (gas-poor) mergers of galaxies (e.g., Begelman et al. 1980; Ebisuzaki et al. 1991; Milosavljević & Merritt 2001; Merritt 2006; Hopkins et al. 2009). Due to only radial orbits being capable of bringing inner stars in close proximity to the SMBH binary, the binary scouring process leaves a relative excess of tangential orbits in the galactic cores (Quinlan & Hernquist 1997; Milosavljević & Merritt 2001; Gebhardt et al. 2003; Thomas et al. 2014, 2016; Rantala et al. 2018). Also, in Dullo & Graham (2015), we found a tendency for the depleted core regions of luminous galaxies to be round. In this paper, we focus on the brightest galaxies, which are expected to host the most massive SMBHs, making them excellent structural probes of extreme cases of core depletion caused by the cumulative actions of massive binary SMBHs.

Earlier studies of depleted cores using ground-based observations lacked the spatial resolution to reveal cores with small angular sizes in enough detail (e.g., King & Minkowski 1966; King 1978; Young et al. 1978; Binney & Mamon 1982; Lauer 1985). The availability of high-resolution *Hubble Space Telescope (HST)* imaging has subsequently allowed us to resolve such small cores and properly characterize depleted cores of "core-Sérsic" galaxies (e.g., Crane et al. 1993; Ferrarese et al. 1994, 2006; Jaffe et al. 1994; Kormendy et al. 1994; van den Bosch et al. 1994; Lauer et al. 1995; Byun et al. 1996; Gebhardt et al. 1996; Faber et al. 1997; Ravindranath et al. 2001; Rest et al. 2001; Graham et al. 2003; Laine et al. 2003; Lauer et al. 2007a, 2007b; Richings et al. 2011; Dullo & Graham 2012, 2013, 2014; Rusli et al. 2013; Dullo et al. 2017). However, as done in a few of

these studies (e.g., Graham et al. 2003; Ferrarese et al. 2006; Dullo & Graham 2012, 2013, 2014; Rusli et al. 2013), reliably determining if a flat inner core in a galaxy actually reflects a deficit of stars relative to the inward extrapolation of the spheroid's outer profile relies on careful modeling of the galaxy light profile using the core-Sérsic model. Applying the core-Sérsic model Dullo & Graham (2012, see also Dullo & Graham 2013) showed that 18 per cent of "cores" according to the Nuker model (Lauer et al. 1995, 2007b) were actually misidentified Sérsic spheroids with low Sérsic indices and no depleted cores (see also Graham et al. 2003; Trujillo et al. 2004; Dullo & Graham 2014). Cores measured using the Nuker model break radii[1] are also typically 2−3 times larger than the core-Sérsic model break radii, R_b, (e.g., Trujillo et al. 2004; Ferrarese et al. 2006; Richings et al. 2011; Dullo & Graham 2012, 2013, 2014). Lauer et al. (2007a, Appendix C) advocated the use of the "cusp radius," i.e., the radius where the negative logarithmic slope of the fitted Nuker model equals 1/2 ($r_{\gamma'=1/2}$, Carollo et al. 1997), as a measure of the core size. While the "cusp radius" somewhat agrees with the core-Sérsic break radius (Dullo & Graham 2012), its application fails to discriminate whether galaxies contain a partially depleted core or not, since all galaxy light profiles have a cusp radius.

In the past few decades, a few papers (e.g., Faber et al. 1997; Lauer et al. 2007a; Rusli et al. 2013; Dullo & Graham 2014; Thomas et al. 2016) have shown strong scaling relations involving the structural parameters of core-Sérsic spheroids. Unfortunately, these scaling relations were established using core-Sérsic spheroids having "normal" size cores (i.e., $R_b \sim 20$–500 pc) and SMBH masses $M_{BH} \lesssim 3 \times 10^9 M_\odot$. The behavior of such scaling relations remains unknown for the most luminous core-Sérsic galaxies with "large" size cores (i.e., $R_b > 0.5$ kpc). In addition, SMBHs with masses of order $10^{10} M_\odot$ are hosted by high-luminosity quasars at high redshift (e.g., Wu et al. 2015) and recent observations have found them in a few extremely massive, present-day galaxies (McConnell et al. 2011; Thomas et al. 2016; Mehrgan et al. 2019). These are important to constrain the SMBH scaling relations at high masses ($M_{BH} \gtrsim 3 \times 10^9 M_\odot$). Given the luminosity function of galaxies (e.g., Efstathiou et al. 1988; Kochanek et al. 2001; Benson et al. 2003; Baldry et al. 2012), it implies that "large-core" galaxies are rare; although, they are becoming increasingly common as more galaxies with high luminosity are modeled (e.g., NGC 6166, Lauer et al. 2007a; 4C +74.13, McNamara et al. 2009; A2261-Brightest Cluster Galaxy (BCG), Postman et al. 2012; Bonfini & Graham 2016; NGC 4486 and NGC 4889, Rusli et al. 2013; NGC 1600, Thomas et al. 2016; A2029-BCG, Dullo et al. 2017; A1689-BCG, Alamo-Martínez & Blakeslee 2017). However, and as noted above, caution should be exercised when interpreting large depleted cores, particularly those identified by the Nuker model (e.g., Lauer et al. 2007a; López-Cruz et al. 2014). For example, López-Cruz et al. (2014) claimed that the BCG Holm 15A has the largest core size measured in any galaxy to date ($r_{\gamma'=1/2} \sim 4.6$ kpc) based on their Nuker model analysis. In contrast, Bonfini et al. (2015) and Madrid & Donzelli (2016) did not identify a central stellar deficit relative to the spheroid's outer Sérsic profile in their modeling of the galaxy's CFHT and Gemini data, respectively, while Mehrgan et al. (2019) fit the 2D core-Sérsic+Sérsic+GaussianRing3D model to their Wendelstein image of the galaxy and reported a core size $R_b \sim 2.8$ kpc.

Accurate extension of the galaxy structural scaling relations to the most massive galaxies carries valuable clues about the supposed joint evolution of SMBHs and their host spheroids. Of particular relevance is the observed correlation between the mass of the SMBH (M_{BH}) and the size of the depleted core (R_b). Absence of a bend/offset in the R_b–M_{BH} relation for the most massive spheroids would imply that the core size is a good predictor of SMBH masses at the high-mass end, more reliable than σ (e.g., Thomas et al. 2016). Lauer et al. (2007a) noted that SMBH masses for the most luminous galaxies are overmassive relative to the inference from the high-mass end of the M_{BH}–σ relation, but they are in better agreement with those from M_{BH}–L relation (see also Volonteri & Ciotti 2013). The M_{BH}–σ relation predicts M_{BH} for the most massive galaxies (i.e., $\sigma \sim 300$–390 km s^{-1}, Bernardi et al. 2007; Lauer et al. 2007a) cannot exceed $M_{BH} \sim 5 \times 10^9 M_\odot$, whereas predicted M_{BH} from the M_{BH}–L relation can surpass $M_{BH} \sim 10^{10} M_\odot$ (Lauer et al. 2007a). The rationale for this discrepancy is that the most massive spheroids are expected to undergo a larger number of dry major mergers that increase their stellar mass, black hole mass, and size, while keeping their velocity dispersion relatively unaffected (e.g., Nipoti et al. 2003; Ciotti et al. 2007; Oser et al. 2012; Hilz et al. 2013). This is also evident from the broken σ–L relation of elliptical galaxies (Faber & Jackson 1976), which displays a shallower slope at bright magnitudes $M_V \lesssim -21.5$ mag ($\sigma \propto L^{1/(5-8)}$, e.g., Malumuth & Kirshner 1981; Lauer et al. 2007a; Kormendy & Bender 2013), whereas at fainter magnitudes $\sigma \propto L^{1/2}$ (e.g., Davies et al. 1983; Held et al. 1992; Matković & Guzmán 2005). This change in the slope of the σ–L relation matches the core-Sérsic versus Sérsic structural divide (e.g., Sahu et al. 2019).

Here, we perform careful, multicomponent (halo/intermediate-scale component/spheroid/nucleus) decompositions of the new light profiles of 12 "large-core" galaxies (i.e., nine BCGs, two second brightest cluster galaxies, and one brightest group galaxy) using a core-Sérsic model and a Sérsic model. Together with the large-core BCG IC 1101 (Dullo et al. 2017), these 13 galaxies constitute the largest sample of "large-core" galaxies studied to date. We aim to revisit the structural scaling relations of our full sample of 41 core-Sérsic galaxies (13 "large-core" galaxies plus 28 "normal-core" galaxies, Dullo & Graham 2014) over a comprehensive dynamic range in core size ($R_b \sim 0.02$–4.2 kpc), spheroid luminosity (-20.70 mag $\gtrsim M_V \gtrsim -25.40$ mag), spheroid stellar mass ($M_* \sim 8 \times 10^{10}$–$7 \times 10^{12} M_\odot$), and SMBH mass ($M_{BH} \sim 2 \times 10^8$–$2 \times 10^{10} M_\odot$).

The paper is organized as follows. Data and photometry for our new sample of 12 large-core galaxies are presented in Section 2. We then discuss the analytical models employed and multicomponent decompositions of these 12 large-core galaxies in Section 3. Accurate structural relations for our full sample of 41 core-Sérsic galaxies are presented in Section 4. We go on to discuss the stellar mass deficits, galaxy environment, and formation of normal- and large-core galaxies in Section 5. Section 6 summarizes our main conclusions. There are two appendices at the end of this paper (Appendices A and B). Appendix A shows the multicomponent decompositions of the new major-axis surface brightness profiles of the 12 large-core galaxies. In Appendix B, we

[1] Graham et al. (2003) revealed that the Nuker model parameters are unstable and deviate from the true values as larger radial extents are probed by the light profile fitting.

Table 1
Global Properties for Our Full Sample of 13 Core-Sérsic Galaxies with Large Break Radii (i.e., $R_b > 0.5$ kpc)

Cluster or Group	BCG or BGG	Type	D (Mpc)	σ (km s^{-1})
(1)	(2)	(3)	(4)	(5)
NGC 1600	NGC 1600	E3	66.0	331
Virgo	NGC 4486†	cD pec	23.0	323
Coma/A1656	NGC 4874†	cD0	106.4	271
Coma/A1656	NGC 4889	cD4	96.6	347(2a)
A2199	NGC 6166	cD2 pec	130.4	300(4a)
MS0735.6+7421	4C +74.13	cD	925.3	239(1a)
A0119	UGC 579	E	185.7	287
A2029	IC 1101	E	363.0	378
A2147	UGC 10143	cD	153.4	276
A2261	A2261-BCG	cD	958.8	387(3a)
A3558	ESO 444-G46	cD4	204.9	248
A3562	ESO 444-G72	SAB(rs)0^0	213.3	236
A3571	ESO 383-G76	cD5	169.0	322

Note. Col. (1): cluster or group name. All of the galaxies in our sample except for the dominant group galaxy NGC 1600 reside in clusters. Col. (2): the superscript "†" denotes the two second brightest cluster elliptical galaxies in the sample that inhabit the centers of their clusters (Figure 1). An alternative designation for A2261-BCG is 2MASX J17222717+3207571. Col. (3): classification came from NED (http://ned.ipac.caltech.edu). Col. (4): distances (D) came from NED (3K CMB), assuming H_0~=~70 km s^{-1} Mpc^{-1}. Col. (5): central velocity dispersions (σ) are taken from HyperLeda (http://leda.univ-lyon1.fr) (Paturel et al. 2003) unless the source is indicated. Sources: (1a) McNamara et al. (2009); (2a) McConnell et al. (2011); (3a) Postman et al. (2012); and (4a) Bender et al. (2015).

show the spatial distribution of large-core galaxies and their nearest neighbors.

Throughout this paper, we assume a cosmology with $H_0 = 70$ km s^{-1} Mpc^{-1}, $\Omega_\Lambda = 0.7$, and $\Omega_m = 0.3$ and quote magnitudes in the Vega system, unless noted otherwise.

2. Data and Photometry

2.1. Sample Selection

We searched the literature for galaxies that were suspected to have a core-Sérsic break radius $R_b > 0.5$ kpc and with archival high-resolution *HST* imaging. This resulted in a selected sample of 13 galaxies (see Table 1). The case of the BCG IC 1101 is published in Dullo et al. (2017) and the remaining 12 galaxies consist of nine galaxies with $r_\gamma > 0.5$ kpc drawn from the Lauer et al. (2007b), 4C +74.13 (McNamara et al. 2009, $r_\gamma = 1.54$ kpc), the BCG of AA2261 (Postman et al. 2012, $r_\gamma = 3.95$ kpc), and the giant cD galaxy NGC 4486 (Richings et al. 2011, $R_b \sim 0.5$ kpc; Rusli et al. 2013, $R_b \sim 0.7$ kpc). Basic data for the full sample of 13 galaxies are listed in Table 1.

Fitting the "sharp-transition" ($\alpha \to \infty$) core-Sérsic model to the inner 10″ *HST* Advanced Camera for Surveys (ACS)/HRC light profiles of 23 massive galaxies, Hyde et al. (2008, their Table 2) measured $R_b > 0.5$ kpc for 5/23 galaxies with high velocity dispersion ($\sigma > 350$ km s^{-1}). These five galaxies are not included here, and we suspect that the sharp-transition core-Sérsic model used by Hyde et al. (2008) may have caused the break radii of the galaxies to be overestimated, as was the case for the BCG SDSS J091944.2+562201.1. Hyde et al. (2008) reported a large break radius of $R_b \sim 1.54$ kpc for this galaxy, which was later found to have a much smaller break radius ($R_b \sim 0.55$ kpc) after fitting a smoother transition (i.e., $\alpha \sim 1.2$) core-Sérsic model to the galaxy's two-dimensional light distribution (Bonfini & Graham 2016). After we completed the analysis in this paper, Alamo-Martínez & Blakeslee (2017) reported a large break radius of 3.8 kpc for the BCG of A1689. We did not include this galaxy in this paper.

2.2. Classification

All of the galaxies in our sample except for three (NGC 1600, NGC 4486, and NGC 4874) are classified as BCGs (Lauer et al. 2007a; Dullo et al. 2017), see Table 1. The elliptical galaxy NGC 1600 is the brightest member of the poor NGC 1600 group. The giant elliptical NGC 4486, which resides at the heart of the Virgo cluster, is the second brightest galaxy in the cluster, only ~0.2 mag fainter than the cluster's brightest elliptical galaxy NGC 4472 (McConnell et al. 2011). Akin to NGC 4486, the giant elliptical NGC 4874 is the second brightest galaxy sitting at the center of the Coma cluster.

2.3. Archival Galaxy Images and Surface Brightness Profiles

We used high-resolution *HST* imaging of the galaxies obtained mainly in the Wide Field Planetary Camera 2 (WFPC2) F814W, ACS WFC F814W/F850LP and Near Infrared Camera and Multi-Object Spectrometer (NICMOS) NIC2 F160W filters in order to minimize the obscuring effects of dust. *HST* WFPC2 F606W images were used for 2/12 galaxies with no obvious dust absorption (NGC 4874 and NGC 4889). These *HST* images were all retrieved from the Hubble Legacy Archive (HLA[2]) and processed through the standard HLA data reduction pipeline. Table 2 lists the *HST* programs, instruments and filters for the sample of 12 galaxies studied in this paper. The *HST* F814W, F850LP, and F160W filters are analog to the Johnson-Cousins *I*-band, *SDSS* z-band, and Johnson-Cousins *H*-band filters, respectively. The full WFPC2 detector is a mosaic of three wide field cameras plus a smaller high-resolution planetary camera, yielding a 160″ × 160″ L-shaped field of view. The mosaic of the two ACS WFC CCD cameras covers a ~202″ × 202″ rhomboidal area. The NIC2 images have a relatively smaller field of view of 19.″2 × 19.″2. The spatial scales of the final processed images are 0.″05, 0.″05 and 0.″1 for the ACS WFC, NICMOS NIC2, and combined WFPC2 images, respectively (Table 2). Figure 1 shows the *HST* images for the 12 sample galaxies.

BCGs[3] and the most luminous elliptical galaxies tend to have extended, low surface brightness stellar envelopes, halos, (Morgan & Lesh 1965; Oemler 1974; Schombert 1986). Therefore, the extraction of accurate surface brightness profiles for such galaxies requires spatially extended images. The high-resolution *HST* ACS WFC images were sufficiently extended in radius to robustly determine the shapes of the outer parts of the light profiles for the two farthest ($D > 925$ Mpc) galaxies in our sample (4C +74.13 and A2261-BCG), Figure 1. For one sample galaxy (A3558-BCG), we extracted a composite surface brightness profile from the ACS/F814W images obtained as a part of the *HST* observing program 10429 under visits 17 and 21 (PI: J. Blakeslee), probing a large range in radius ($R \sim 150''$).

For the remaining 9/12 sample galaxies (NGC 1600, NGC 4486, NGC 4874, NGC 4889, NGC 6166, A0119-BCG,

[2] https://hla.stsci.edu

[3] For BCGs, the faint stellar envelopes are due to the intracluster light (ICL).

Table 2
Data Source

Galaxy	*HST* Program	*HST* Filter	*HST* Image Scale (arcsec pixel^{-1})	Data at Large Radii	Field of View (arcmin)
(1)	(2)	(3)	(4)	(5)	(6)
NGC 1600	7886	NICMOS/F160W	0.″05	CGS *I*-band	8.90 × 8.90
NGC 4486	10543	ACS/F814W	0.″05	SDSS *i*-band	13.52 × 9.83
NGC 4874	6104	WFPC2/F606W	0.″10	SDSS *r*-band	13.52 × 9.83
NGC 4889	5997	WFPC2/F606W	0.″10	SDSS *r*-band	13.52 × 9.83
NGC 6166	9293	ACS/F814W	0.″05	SDSS *i*-band	13.52 × 9.83
4C +74.13	10495	ACS/F850LP	0.″05	...	...
A0119-BCG	8683	WFPC2/F814W	0.″10	SDSS *i*-band	13.52 × 9.83
A2147-BCG	8683	WFPC2/F814W	0.″10	SDSS *i*-band	13.52 × 9.83
A2261-BCG	12066	ACS/F850LP	0.″05	...	...
A3558-BCG	10429	ACS/F814W	0.″05	*HST* ACS/F814W	3.37 × 3.37
A3562-BCG	8683	WFPC2/F814W	0.″10	2MASS *J*-band	8.53 × 17.07
A3571-BCG	10429	ACS/F814W	0.″05	2MASS *J*-band	8.53 × 17.07

Note. Space- and ground-based imaging used for our sample of 12 extremely massive galaxies with $R_b > 0.5$ kpc (i.e., "large-core galaxies"). Col. (1): galaxy name. Col. (2): *HST* programs. Program ID: GO-5997 (PI: J. Lucey); GO-6104 (PI: W. Harris); GO-7886 (PI: A. Quillen); GO-8683 (PI: R. van der Marel); GO-9293 (PI: H. Ford); GO-10429 (visits 17 and 21, PI: J. Blakeslee); GO-10495 (PI: B. McNamara); GO-10543 (PI: E. Baltz); and GO-12066 (PI: M. Postman). Cols. (3) and (4): *HST* filters and image scales. Cols. (5) and (6): data at large radii and the associated field of view. For NGC 1600, we combine the inner *HST* F160W/NICMOS NIC2 light profile ($R \lesssim 4''$) with the ground-based, Carnegie-Irvine Galaxy Survey (CGS) *I*-band data at $R > 4''$ obtained using the du Pont 2.5 m telescope (Li et al. 2011). For A3558-BCG, we used ACS/F814W images obtained as a part of the *HST* observing program 10429 under visits 17 and 21 (PI: J. Blakeslee).

A2147-BCG, A3562-BCG, and A3571-BCG), the high-resolution *HST* NICMOS, WFPC2, and ACS images were limited in radius to accurately describe the outer part of the galaxies' light profiles and to perform reliable sky background subtraction (see Figure 1). These galaxies' *HST* light profiles at small radii (i.e., typically $R \lesssim 40''$) were matched with low-resolution, ground-based data at larger radii ($R > 40''$) determined from extended images from the SDSS[4] and 2MASS archives[5] (see Table 2). An exception is NGC 1600, where we combine the high-resolution *HST* profile at small radii ($R \lesssim 4''$) with ground-based surface brightness profile at large radii ($R > 4''$) that was extracted by Li et al. (2011) from extended *I*-band images obtained with the du Pont 2.5 m telescope. When possible, we used *HST* and ground-based images taken with similar filters. This was not the case for NGC 1600, A3562-BCG, and A3571-BCG, where we matched light profiles extracted from images obtained using different filters (Table 2, see also Lauer et al. 2007a; Thomas et al. 2016). We find an excellent overlap between the *HST* light profiles of the galaxies and the corresponding ground-based data over the $R \sim 2''$–$60''$ radial range, except for NGC 1600 where the overlap between the *HST* and ground-based data is over $R \sim 2''$–$6''$.

The full details of our data reduction steps and the surface brightness profile extraction techniques are given in Dullo et al. (2017, 2018). The extraction of accurate surface brightness profiles depends on the careful masking of the bright foreground stars, low-luminosity neighboring and background galaxies, and chip defects in the image. Initial masks were generated for the galaxies by running SEXTRACTOR (Bertin & Arnouts 1996), which were then complemented with manual masks. We follow the steps in Dullo et al. (2019) to subtract the model images of the target galaxies from the science images and to improve our initial masks. The composite surface brightness (μ) and ellipticity (ϵ) profiles of the full sample galaxies, extracted using the IRAF task ELLIPSE (Jedrzejewski 1987), are available in Appendix A. Given that we shift the ground-based profiles to the match *HST* data, the composite surface brightness profiles are given in their respective *HST* filters (Figure 1 and Appendix A).

We quote all magnitudes in the VEGA magnitude system.

3. Light Profile Modeling of BCGs and Central Dominant Galaxies

As noted above, BCGs and the most luminous elliptical galaxies tend to exhibit faint stellar envelopes at large radii. This is evident by a light excess in their outer light distribution with respect to the de Vaucouleurs (1948) $R^{1/4}$ model, which is fit to the spheroidal[6] components of the galaxies (e.g., Oemler 1974; Carter 1977; Dressler 1981; Lugger 1984; Schombert 1986; Gonzalez et al. 2003, 2005; Zibetti et al. 2005).

The Sérsic (1963, 1968) $R^{1/n}$ model describes the stellar light distributions of faint and intermediate-luminosity ($M_B \gtrsim -20.5$ mag) spheroids (see Dullo & Graham 2012; Dullo et al. 2016, 2019). This model is written as

$$I(R) = I_e \exp\left\{-b_n\left[\left(\frac{R}{R_e}\right)^{1/n} - 1\right]\right\}, \quad (1)$$

where I_e is the intensity at the half-light (effective) radius (R_e). The quantity $b_n \approx 2n - 1/3$ for $1 \lesssim n \lesssim 10$ (Caon et al. 1993) is expressed as a function of the Sérsic index n, and ensures that R_e encloses half of the total luminosity. For $n = 0.5$ and 1, the Sérsic model is a Gaussian function and an exponential function, respectively.

The surface brightness profiles of luminous ($M_B \lesssim 20.5$ mag) spheroids are well described by the core-Sérsic model, which is a combination of an inner power-law core and an outer Sérsic

[4] https://www.sdss.org
[5] https://irsa.ipac.caltech.edu/Missions/2mass.html

[6] The term "spheroid" is used here to refer to the underlying host galaxy in case of elliptical galaxies and the bulge for disk galaxies.

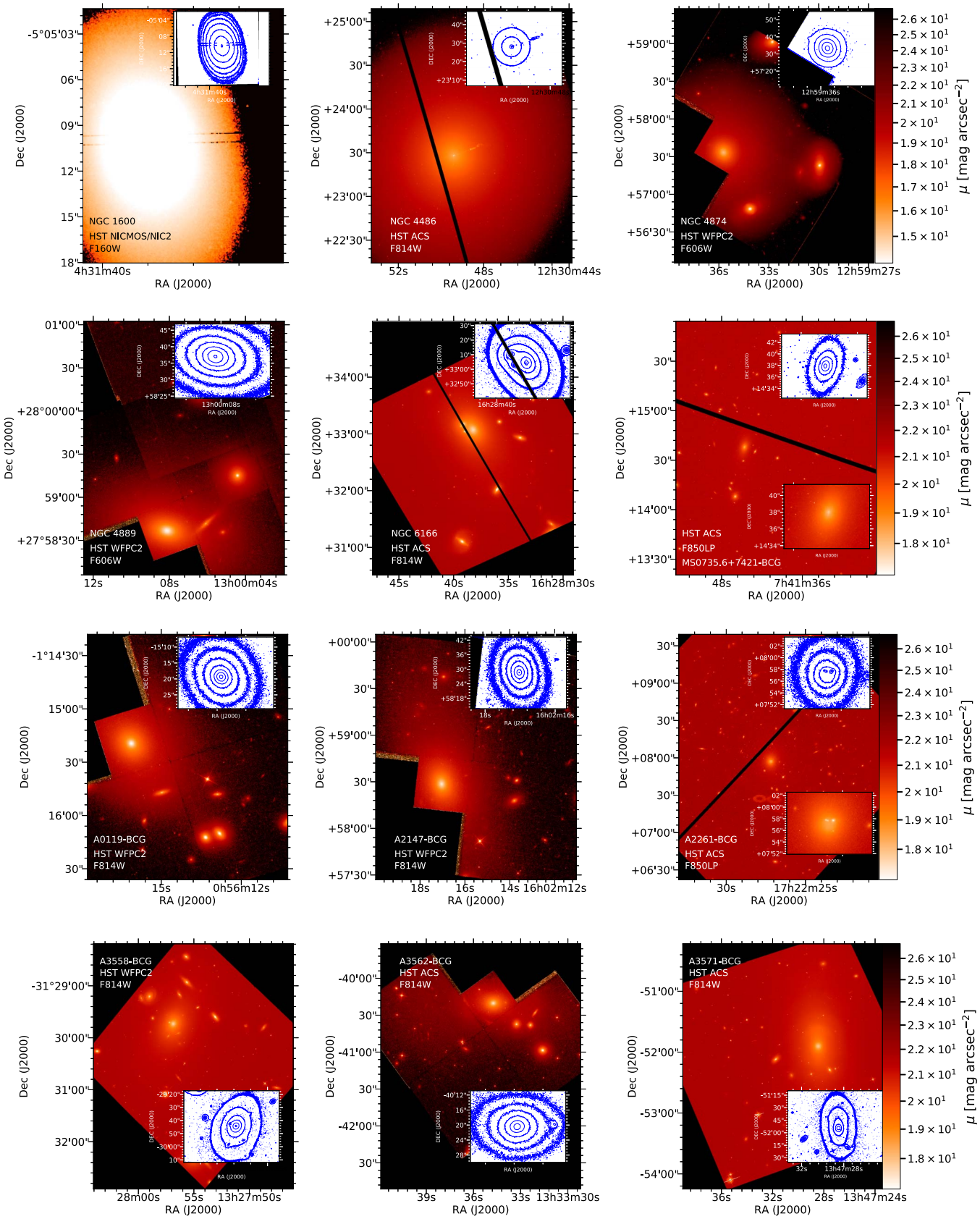

Figure 1. *HST* images of our sample of 12 massive galaxies with large break radii $R_b > 0.5$ kpc (Tables 2 and 3). The insets show the contour levels in steps of 0.6 mag arcsec^{-2}. For 4C +74.13 and A2261-BCG, we show zoomed-in regions centered on the BCGs. North is up and east is to the left.

profile with a transition region (Graham et al. 2003; Trujillo et al. 2004). This model, discussed in detail in Dullo & Graham (2012), is given by

$$I(R) = I'\left[1 + \left(\frac{R_{\rm b}}{R}\right)^{\alpha}\right]^{\gamma/\alpha} \exp\left[-b\left(\frac{R^{\alpha} + R_{\rm b}^{\alpha}}{R_{\rm e}^{\alpha}}\right)^{1/(\alpha n)}\right], \quad (2)$$

with

$$I' = I_{\rm b} 2^{-\gamma/\alpha} \exp\left[b(2^{1/\alpha} R_{\rm b}/R_{\rm e})^{1/n}\right], \quad (3)$$

where $I_{\rm b}$ is intensity at the core break radius $R_{\rm b}$, γ is the slope of the inner power-law region, and α regulates the sharpness of the transition between the inner power-law core and the outer Sérsic profile. The parameters $R_{\rm e}$ and b are defined as in the Sérsic model.

3.1. Multicomponent Decomposition of Large-core Galaxies

In Dullo et al. (2017), the 1D and 2D decompositions of the high-resolution *HST* F702W and F450W data of the BCG IC 1101 revealed a Sérsic intermediate-scale component, an outer exponential halo and an inner Gaussian component that are additional to the core-Sérsic spheroid light distribution. This galaxy has the largest core size measured in any galaxy to date ($R_{\rm b} \sim 4.2$ kpc). Following Dullo et al. (2017), we fit, here, the major-axis surface brightness profiles of the remaining 12 "large-core" (i.e., $R_{\rm b} > 0.5$ kpc) core-Sérsic galaxies (Table 1) using a point-spread function (PSF)-convolved core-Sérsic model. Figure 13 shows the fit residual profiles and the corresponding root-mean-square (rms) residual values (Δ). A single core-Sérsic model was adequate only for two of the 12 sample galaxies (NGC 4889 and A3558-BCG). Additional nuclear light components (i.e., active galactic nucleus (AGN) or nuclear star clusters) were identified in three sample galaxies (NGC 4486, NGC 6166, and A2147-BCG) and were modeled using a Gaussian or a Sérsic model. Of the 12 sample galaxies, nine have an outer stellar halo light, which was well described by an exponential function. We find that the light profiles for two sample galaxies (NGC 4874 and A3571-BCG) are well described by a core-Sérsic spheroid, a Sérsic intermediate-scale component and an outer exponential halo model. In Section 5.3, we show that the colors for these two objects gradually turn bluer toward larger radii, consistent with our multicomponent light profile decompositions. In addition, Veale et al. (2017) showed that the velocity dispersion of NGC 4874 increases outward from 240 km s^{-1} near the center to 350 km s^{-1} at $R \sim 60''$, akin to that of the large-core galaxy IC 1101 having an intermediate-scale component. We also note that Seigar et al. (2007) modeled the *R*-band ground-based data of NGC 4874 with poor seeing conditions ($\sim 1\farcs5$), excluding the inner $\sim 3''$ data points, using a Sérsic spheroid plus a de Vaucouleurs stellar halo model. Due to the intermediate-scale component of the galaxy, which was missed in the Seigar et al. (2007) modeling, their fit resulted in an incorrect, high Sérsic index ($n = 4$) for the outer exponential halo.

The best-fitting parameters are determined by iteratively minimizing the rms residuals using the Levenberg–Marquardt optimization algorithm (Dullo et al. 2017). For each iteration, the profiles of individual model components were convolved with the Gaussian PSF and then summed to create the final model profile. Our PSF implementation is as in Dullo et al. (2017). The full widths at half-maximum of the PSFs have been measured from bright stars in the *HST* images of the galaxies. Trujillo et al. (2001) noted that Moffat functions are numerically better suited for modeling the PSFs in *HST* images than Gaussian functions when the inner galaxy light profiles are steep. Fitting both Gaussian and Moffat PSF-convolved models to the *HST* light profiles of the BCG IC 1101 with a flat (i.e., an inner slope $\gamma \leqslant 0.05$–0.08) depleted core, Dullo et al. (2017) however showed that the best-fitting structural parameters remain unchanged irrespective of the choice of PSF. This should also be the case for the bulk (10/12) of our sample galaxies with flat cores (i.e., $\gamma \lesssim 0.15$). While the remaining two galaxies NGC 4486 and 4C +74.13 have $\gamma > 0.15$, our Gaussian PSF-convolved models give excellent fits to the galaxies' *HST* profiles (Appendix A). However, we admit the possibility that the inner Sérsic model component of NGC 4486 may be a poor fit to the nuclear source in the galaxy.

3.2. Spheroid Magnitudes and Stellar Masses

The total integrated spheroid fluxes for the sample galaxies were computed using the best-fitting major-axis, core-Sérsic structural parameters and the ellipticities of the spheroids (Table 3 and Figure 14). We corrected these magnitudes for foreground Galactic extinction using reddening values taken from NED (Schlafly & Finkbeiner 2011). The magnitudes were also corrected for $(1+z)^4$ surface brightness dimming. To compare directly with previously published magnitudes (Lauer et al. 2007a; McNamara et al. 2009; Postman et al. 2012; Dullo & Graham 2014; Dullo et al. 2017), our magnitudes are converted into the *V*-band vega magnitudes (see Table 3). To achieve this, first we extracted light profiles of five sample galaxies from archival *HST* images obtained in the *V*-band filter or filters closer to the *V*-band—NGC 4486, ACS/F606W (GO-10543, PI: E. Baltz); NGC 6166, WFPC2/F555W (GO-7265, PI: D. Geisler); A2261-BCG, ACS/F606W (GO-12066, PI: M. Postman); A3571-BCG, ACS/F475W (GO-10429, PI: J. Blakeslee); A3558-BCG, ACS/F475W (GO-12238, PI: W. Harris). Next, the total integrated magnitudes in the corresponding filters, calculated in the same manner as noted above, were converted into the *V*-band magnitudes, when necessary using Fukugita et al. (1995, their Table 3), see Table 3. For the two most distant galaxies in our sample (MS0735-BCG and A2261-BCG), evolution- and *K*-corrections were performed utilizing the values reported in the literature (McNamara et al. 2009; Postman et al. 2012). Furthermore, the galaxy distances in Lauer et al. (2007b), McNamara et al. (2009), and Postman et al. (2012) are somewhat different from those adopted here (see Table 1). Therefore, we adjusted the magnitudes from the literature to our distances.

We convert the spheroid luminosities (L) into stellar masses (M_*) using stellar mass-to-light (M/L) ratios, which are obtained from Worthey (1994) assuming an old ($\sim$12 Gyr) stellar population (see Table 5).

3.3. Comparison to Previous Fits

Here, we compare the values of our core-Sérsic $R_{\rm b}$ and M_V with those from the literature for the 12 galaxies (Table 3) and discuss notable discrepancies (see Figure 2). It should be noted that this work has, for the first time, modeled the light profiles for full sample of 12 galaxies using a core-Sérsic model.

Table 3
Best-fitting Core-Sérsic Parameters for Our Large-core Galaxies

Galaxy	Type	*HST* Filter	μ_b (mag arcsec^{-2})	R_b (arcsec)	R_b (kpc)	γ	α	n	R_e (arcsec)	R_e (kpc)	ϵ_b	M_{uncorr} (mag)	M_{corr} (mag)	ΔM	$M_{V,corr}$ (mag)
(1)	(2)	(3)	(4)	(5)	(6)	(7)	(8)	(9)	(10)	(11)	(12)	(13)	(14)	(15)	(16)
NGC 1600	E	F160W/NICMOS	15.14	2.08	0.65	0.04	2	6.3	72.6	22.8	0.270	−26.53	−26.61	2.95	-23.66
NGC 4486	E†	F814W/ACS	16.41	5.80	0.64	0.24	5	6.2	185.9	20.6	0.021	−24.86	−24.92	1.33	−23.59
NGC 4874	E†	F606W/WFPC2	19.05	3.25	1.63	0.13	2	4.0	4.9	2.5	0.099	−22.06	−22.18	0.33	−21.85
NGC 4889	BCG	F606W/WFPC2	17.68	1.89	0.86	0.04	2	13.3	563.9	256.7	0.065	−25.54	−25.66	0.33	−25.33
NGC 6166	BCG	F814W/ACS	18.26	3.46	2.11	0.05	2	9.0	136.5	83.1	0.135	−25.80	−25.95	1.33	−24.62
4C +74.13	BCG	F850LP/ACS	18.83	0.64	2.24	0.28	2	3.7	6.0	20.9	0.100	−25.00	−25.76	1.64	−24.12
A0119-BCG	BCG	F814W/WFPC2	17.34	0.78	0.67	0.10	5	6.8	112.5	96.1	0.074	−25.58	−25.82	1.31	−24.51
A2147-BCG	BCG	F814W/WFPC2	18.09	1.79	1.28	0.14	2	6.4	44.6	31.8	0.180	−24.73	−24.92	1.31	−23.61
A2261-BCG	BCG	F850LP/ACS	18.69	0.75	2.71	0.00	5	2.1	4.9	17.6	0.036	−25.33	−26.34	1.80	−24.54
A3558-BCG	BCG	F814W/ACS	18.08	1.39	1.30	0.03	2	5.4	131.9	123.7	0.029	−26.45	−26.73	1.33	−25.40
A3562-BCG	BCG	F814W/WFPC2	17.66	0.66	0.64	0.06	2	3.6	18.9	18.4	0.099	−24.44	−24.73	1.31	−23.42
A3571-BCG	BCG	F814W/ACS	18.56	1.70	1.33	0.01	2	10.2	68.9	53.8	0.062	−24.47	−24.72	1.37	−23.35

Note. Structural parameters from the core-Sérsic model fits to the major-axis surface brightness profiles of the spheroids of our large-core galaxies. Col. (1) galaxy name. The superscript "†" indicates the two second brightest cluster elliptical galaxies in the sample. Col. (2) morphological type. Col. (3) *HST* filters and instruments. Cols. (4−11) best-fitting core-Sérsic model parameters. Col. (12) galaxy ellipticity at the break radius R_b. Col. (13) spheroid absolute magnitudes derived using our fit parameters (cols. 4−11). Spheroid magnitudes corrected for Galactic dust extinction using NED (Schlafly & Finkbeiner 2011), and $(1+z)^4$ surface brightness dimming are given in col. (14). For 4C +74.13 and A2261-BCG, we also carried out evolution- and *K*-corrections using the values taken from McNamara et al. (2009) and Postman et al. (2012), respectively. Col. (15) ΔM = (*HST* filter)-*V*. Col. (16) corrected, *V*-band spheroid absolute magnitude. We estimate that the uncertainties on the core-Sérsic parameters R_b, γ, n, and R_e are ∼2.5%, 10%, 20%, and 25%, respectively. The uncertainty on μ_b is ∼0.02 mag arcsec^{-2}. These errors on the fit parameters were estimated following the techniques in Dullo et al. (2019, their Section 3.1).

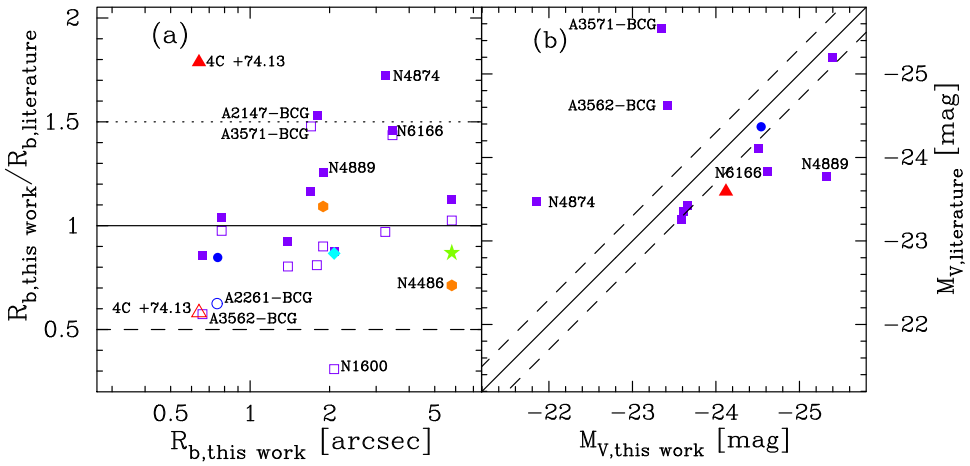

Figure 2. Left panel: comparison of our core-Sérsic break radii (Table 3) and the cusp radii (r_γ), Nuker break radii and core-Sérsic break radii from the literature (Lauer et al. 2007b; McNamara et al. 2009; Richings et al. 2011; Postman et al. 2012; Rusli et al. 2013; Thomas et al. 2016). For 4C +74.13, the McNamara et al. (2009) Nuker break radius is converted to r_γ using their Nuker model fit parameters. The filled (and open) boxes are the cusp (and Nuker break) radii for galaxies in common with Lauer et al. (2007b). The filled (and open) triangle and circle denote the cusp (and Nuker break) radii for 4C +74.13 (McNamara et al. 2009) and A2261-BCG (Postman et al. 2012), respectively (See Section 3.3). The filled hexagons are the core-Sérsic break radii for NGC 4486 and NGC 4889 from Rusli et al. (2013), whereas the filled diamond and star denote the core-Sérsic break radii for NGC 1600 (Thomas et al. 2016) and NGC 4486 (Richings et al. 2011), respectively. Right panel: comparison of our absolute V-band spheroid magnitudes M_V (Table 3) with previous spheroid magnitudes in the literature. We adjusted the absolute magnitudes from the literature using our distances given in Table 1 (see the text for further detail). The solid line is a one-to-one relation, while the dashed lines are $M_{V,\mathrm{literature}} = M_{V,\mathrm{thiswork}} \pm 0.30$ mag. Symbolic representations are as in panel (a).

In general, the core-Sérsic break radii are in fair agreement with the cusp radii, but there are five discrepant data points (Figure 2(a)). Our core-Sérsic break radii are ($\gtrsim$25%) larger than the cusp radii reported for four galaxies in common with Lauer et al. (2007b), NGC 4874, NGC 4889, NGC 6166, and A2147-BCG, and for 4C +74.13 (McNamara et al. 2009). For comparison, the 1σ uncertainty range of R_b adopted in this paper is 2.5%. We believe the discrepancies in the break radii arise from differences in the (1) fitting models employed, (2) fitted radial extent of the galaxy light profiles, and (3) treatment of distinct galaxy structural components. Our break radii are obtained from careful, multicomponent (halo/intermediate-scale component/spheroid/nucleus) decompositions of spatially extended (i.e., typically $R \gtrsim 100''$) light profiles. In contrast, Lauer et al. (2007b, and references therein) and McNamara et al. (2009) determined the cusp radii fitting the Nuker model to their $10''$ galaxy light profiles, without accounting for any additional light components.

As noted in the Introduction, the Nuker break radii poorly match the core-Sérsic break radii (see Figure 2(a)). Of the 10 galaxies in common with Lauer et al. (2007b), six (NGC 1600, NGC 6166, A2147-BCG, A3558-BCG, A3562-BCG, and A3571-BCG) have Nuker break radii that differ from our core-Sérsic R_b by more than 25%. Also, the Nuker break radii for 4C+74.13 (McNamara et al. 2009) and A2261-BCG (Postman et al. 2012) are roughly 65% larger than our R_b values. We note that the Nuker[7] break radii tend to be bigger (smaller) than our core-Sérsic break radii for spheroids with a Sérsic index $n \lesssim 6$ ($n \gtrsim 9$).

We have also included a comparison of our break radii with those from similar studies in the literature, which performed core-Sérsic model fits (Figure 2(a), NGC 4486, Richings et al. 2011; NGC 4486 and NGC 4889, Rusli et al. 2013; NGC 1600, Thomas et al. 2016). The agreement between our core-Sérsic break radii and those from the literature is remarkably good, except for the break radius of NGC 4486 (Rusli et al. 2013), which is ~40% larger than ours. It appears that the Rusli et al. (2013) $R_\mathrm{b} \sim 8\farcs14$ and $n \sim 8.9$ for NGC 4486are biased high due to the outer halo light of the galaxy that was not separately modeled. While Kormendy et al. (2009) identify excess halo light at large radii ($R \sim 400''$–$1000''$) with respect to their Sérsic model fit to the main body of the NGC 4486, Rusli et al. (2013) fit the core-Sérsic model to the entire radial extent ($R \sim 1000''$) of the galaxy light profile from Kormendy et al. (2009). We find that our $R \sim 400''$ light profile for the galaxy is better described using a core-Sérsic model for spheroid plus a Gaussian function for the AGN (Figure 13); this fit yields $R_\mathrm{b} \sim 5\farcs80$ and $n \sim 6.2$.

Figure 2(b) shows our magnitudes (Table 3) disagree with those from past works (Lauer et al. 2007a; McNamara et al. 2009; Postman et al. 2012), by typically more than ~0.30 mag. Our spheroid luminosities are brighter than those from Lauer et al. (2007b) for seven of the 10 galaxies that we have in common (NGC 1600, NGC 4486, NGC 4889, NGC 6166, A0119-BCG, A2147-BCG, and A3558-BCG). This discrepancy arises primarily because all seven galaxies have spheroids with $n > 4$ (Table 3). For "regular" elliptical galaxies, Lauer et al. (2007a, their Section 2.1) used total V_T or B_T galaxy magnitudes from the Third Reference Catalogue of Bright Galaxies RC3 (de Vaucouleurs et al. 1991), which are determined by fitting the galaxy light profiles using the de Vaucouleurs (1948) $R^{1/4}$ function (i.e., $n = 4$ Sérsic model). For BCGs, Lauer et al. (2007a) estimated the spheroid luminosities fitting the $R^{1/4}$ model to the inner $R \lesssim 50$ kpc light profiles and they argued that the halo light contribution to the BCGs' light profiles over the fitted radial extents was insignificant. However, we find three BCGs in common with Lauer et al. (2007a), A2147-BCG, A3562-BCG, and A3571-BCG, where the outer halo light contributes inside $R \sim 50$ kpc (Appendix A). This in part has caused the Lauer et al. (2007a) spheroid magnitudes for A3562-BCG and A3571-BCG to be

[7] The Sérsic $R^{1/n}$ model can approximate a power-law profile for large values of n. This means that the surface brightness distributions of some BCGs with large n may be well described by a core-Sérsic model and also by a Nuker model (e.g., see Graham et al. 2003).

Table 4
Parameters Associated with Additional Light Components

Galaxy	*HST* Filter	$\mu_{0,h}/\mu_{e,S}$ (mag arcsec^{-2})	$h/R_{e,S}$ (arcsec)	n_S	ϵ_h/ϵ_S	m_{pt} (mag)	$m_{h,uncorr}/m_{S,uncorr}$ (mag)	$M_{h,corr}/M_{S,corr}$ (mag)	$M_{V,h}/M_{V,S}$ (mag)
(1)	(2)	(3)	(4)	(5)	(6)	(7)	(8)	(9)	(10)
NGC 1600	F160W/NICMOS	20.14/⋯	29.1/⋯	⋯	0.30/⋯	⋯	11.21/	−22.97/	−20.02/⋯
NGC 4486	F814W/ACS	⋯/⋯	⋯/⋯	⋯	⋯/⋯	15.9	⋯/⋯	⋯/⋯	⋯/⋯
NGC 4874	F606W/WFPC2	23.56/23.2	175.3/46.5	0.80	0.2/0.00	⋯	10.59/12.48	−24.67/−22.78	−24.34/−22.45
NGC 4889	F606W/WFPC2	⋯/⋯	⋯/⋯	⋯	⋯/⋯	⋯	⋯/⋯	⋯/⋯	⋯/⋯
NGC 6166	F814W/ACS	23.22/13.44	110.2/0.02	0.66	0.40/0.00	⋯	11.57/19.60	−24.16/-16.12	−22.83/-14.79
4C 74.13	F850LP/ACS	23.53/⋯	43.3/⋯	⋯	0.50/⋯	⋯	14.11/⋯	−26.49/⋯	−24.85/⋯
A0119-BCG	F814W/WFPC2	23.24/⋯	82.4/⋯	⋯	0.32/⋯	⋯	12.08/⋯	−24.50/⋯	−23.19/⋯
A2147-BCG	F814W/WFPC2	22.75/⋯	85.1/⋯	⋯	0.50/⋯	20.2	11.86/	−24.27/⋯	−22.96/⋯
A2261-BCG	F850LP/ACS	22.30/⋯	20.7/⋯	⋯	0.20/⋯	⋯	13.97/⋯	−26.95/⋯	−25.15/⋯
A3558-BCG	F814W/ACS	⋯/⋯	⋯/⋯	⋯	⋯/⋯	⋯	⋯/⋯	⋯/⋯	⋯/⋯
A3562-BCG	F814W/WFPC2	22.22/⋯	68.9/⋯	⋯	0.50/⋯	⋯	11.79/⋯	−25.16/⋯	−23.85/⋯
A3571-BCG	F814W/ACS	21.17/21.05	373.0/25.3	0.54	0.60/⋯	⋯	7.31/12.23	−29.08/−24.16	−27.71/−22.79

Note. Structural parameters for additional light components. Col. (1) galaxy name. Col. (2) *HST* filters and instruments. Cols. (3–5) best-fitting parameters of the exponential halo/Sérsic model component. Cols. (6) ellipticity of the halo/Sérsic model component. Col. (7) apparent magnitude of the nucleus. Col. (8) apparent halo/Sérsic magnitude derived using our best-fitting exponential/Sérsic model parameters (cols. 3–6). Col. (9) absolute halo/Sérsic model component magnitude corrected for Galactic dust extinction and $(1+z)^4$ surface brightness dimming. For 4C +74.13 and A2261-BCG, we also carried out evolution- and *K*-corrections using the values taken from McNamara et al. (2009) and Postman et al. (2012), respectively. Col. (10) corrected, *V*-band halo/Sérsic model component absolute magnitude.

brighter than ours. Not surprisingly, the Lauer et al. (2007a) spheroid magnitudes for the two galaxies in the sample with an intermediate light component (NGC 4874 and A3571-BCG) are brighter than ours (see Tables 3 and 4).

4. Scaling Relations for Core-Sérsic Galaxies

Luminous early-type galaxies are known to exhibit tight scaling relations involving their central and global structural parameters (e.g., Faber et al. 1997; Dullo & Graham 2012, 2014; Rusli et al. 2013; Thomas et al. 2016). Rusli et al. (2013) investigated the correlation between the core-Sérsic break radius (R_b) and the velocity dispersion, spheroid absolute magnitude and SMBH mass for a sample of 23 core-Sérsic elliptical galaxies with $R_b \lesssim 0.8$ kpc. In Dullo & Graham 2014, we explored a number of scaling relations involving R_b and the break surface brightness (μ_b) for a sample of 28 core-Sérsic early-type spheroids with $R_b \lesssim 0.5$ kpc and -20.70 mag $\gtrsim M_V \gtrsim -23.60$ mag. In this paper, we combine these 28 core-Sérsic spheroids with $R_b \lesssim 0.5$ kpc and $8\times10^{10} \lesssim M_* \lesssim 10^{12} M_\odot$ (henceforth "normal-core spheroids," Dullo & Graham 2014) and the 13 extremely massive spheroids ($M_* \gtrsim 10^{12} M_\odot$) with $R_b \gtrsim 0.5$ kpc and $M_V \lesssim -23.50 \pm 0.10$ mag (henceforth "massive large-core spheroids," Tables 1 and 3) to explore whether or not extremely massive, large-core spheroids adhere to the structural scaling relations established by the relatively less massive, normal-core spheroids. Our 41(=28+13) galaxies represent the hitherto largest sample of core-Sérsic galaxies with detailed multi-component decompositions of the high-resolution, extended light profiles.

4.1. Structural Correlations with the Core's Size: Large-core versus Normal-core Spheroids

Figure 3 shows a compilation of major-axis core-Sérsic model profiles for the 41 core-Sérsic spheroids (see also Appendix A). Also shown in this figure is a strong correlation between R_b and μ_b with Pearson correlation coefficient $r \sim 0.97$ (see also Faber et al. 1997; Lauer et al. 2007a). We find that our massive large-core spheroids follow the tight R_b–μ_b sequence defined by the relatively less massive normal-core spheroids (Table 6).

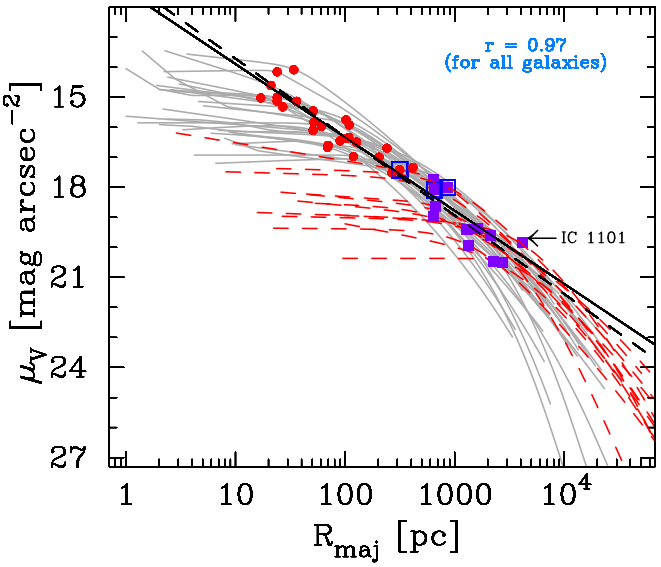

Figure 3. Core-Sérsic fits to the major-axis surface brightness profiles of 28 +13(=41) core-Sérsic galaxies (solid and dashed curves). Filled red circles mark the core-Sérsic break radii (R_b) of the 28 core-Sérsic early-type galaxies with $R_b < 0.5$ kpc (Dullo & Graham 2014, their Table 2). Filled purple boxes indicate the break radii for the 13 core-Sérsic galaxies with $R_b > 0.5$ kpc (i.e., the 12 core-Sérsic galaxies from this work, Table 3, plus IC 1101, Dullo et al. 2017). Blue squares enclose the three galaxies (NGC 3842, NGC 1600, and NGC 4889) with directly measured SMBH masses $M_{BH} \gtrsim 10^{10} M_\odot$ (McConnell et al. 2011; Thomas et al. 2016). The dashed line is a symmetric least-squares fit to the (R_b, μ_b) data set for the full sample of 41 core-Sérsic galaxies, while the solid line is a least-squares fit the 28 core-Sérsic early-type galaxies with $R_b < 0.5$ kpc (Dullo & Graham 2014). The correlation between R_b and μ_b for the 41 core-Sérsic galaxies is extremely strong, with Pearson correlation coefficient $r \sim 0.97$.

In Figure 4, we expand on Figure 6(a) from Dullo & Graham (2014) and plot the relation between the core-Sérsic break

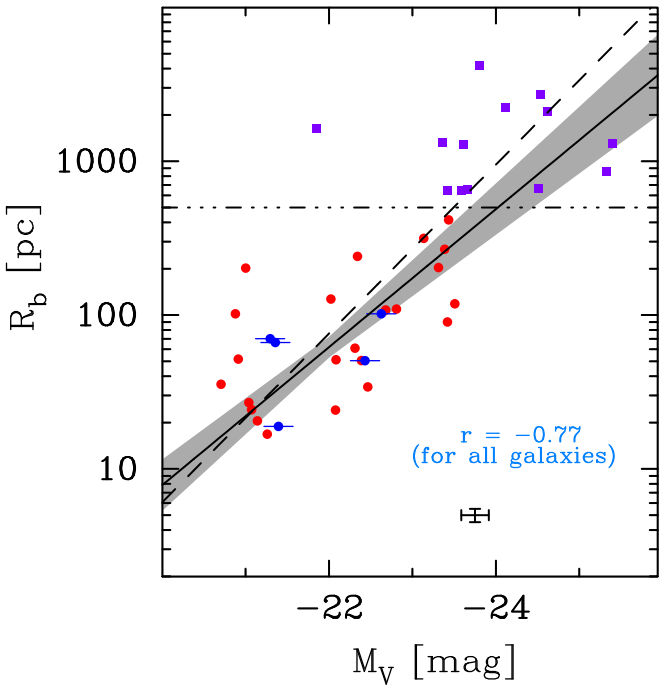

Figure 4. Correlation between the core-Sérsic break radius (R_b) and V-band spheroid absolute magnitude (M_V) for our sample of 41 core-Sérsic galaxies. Filled red circles and disk symbols show the 23 core-Sérsic elliptical galaxies and 5 core-Sérsic S0 galaxies, respectively, with $R_b < 0.5$ kpc (Dullo & Graham 2014, their Table 2), while filled purple boxes indicate the 13 core-Sérsic galaxies with $R_b > 0.5$ kpc (i.e., the 12 core-Sérsic galaxies from this work, Table 3, plus IC 1101, Dullo et al. 2017). The horizontal, dashed-dotted line indicates the $R_b = 0.5$ kpc demarcation. The dashed line is a symmetric least-squares fit to the 41 core-Sérsic galaxies, while the solid line is a symmetric OLS fit to the 28 "normal-core" galaxies (Dullo & Graham 2014). The shaded region shows the 1σ uncertainty on the regression fit. Pearson correlation coefficient (r) and representative error bars for the 41 core-Sérsic galaxies are shown at the bottom.

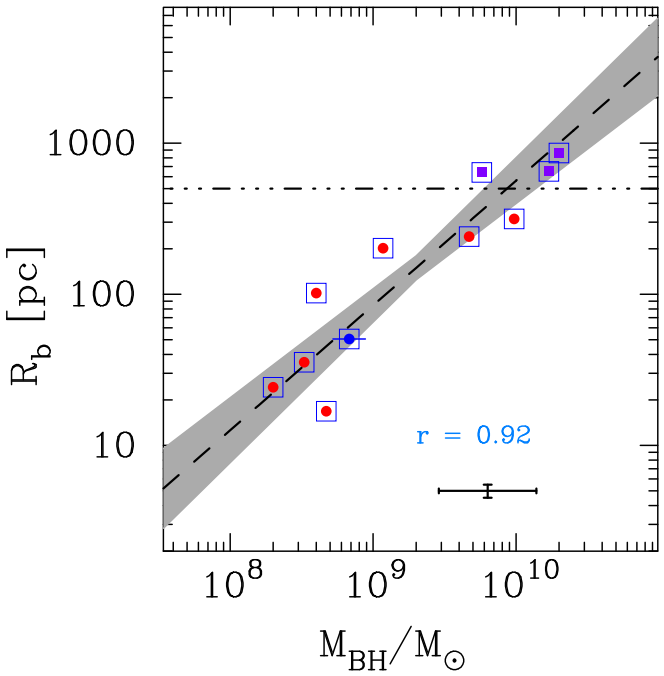

Figure 5. Similar to Figure 4, but showing here the correlation between core-Sérsic break radius (R_b) and SMBH mass (M_{BH}) for 11 galaxies in our sample with directly measured M_{BH}. The dashed line shows our symmetric OLS fit.

radius (R_b) and V-band spheroid absolute magnitude (M_V). The dashed and solid lines are ordinary least-squares (OLS) bisector regression fits (Feigelson & Babu 1992) to the (R_b, M_V) data set for the full sample of 41 core-Sérsic spheroids and the 28 normal-core spheroids, respectively. Because our full galaxy sample spans a wider range in M_V than that of Dullo & Graham (2014), the new, well constrained R_b–L_V relation for the full sample ($R_b \propto L_V^{1.38\pm0.13}$) has a slope ∼22% steeper than the near-linear relation for the normal-core galaxies alone ($R_b \propto L_V^{1.13\pm0.13}$, Dullo & Graham 2014). It is worth noting that the larger cores of extremely massive galaxies are consistent with these galaxies' extremely bright spheroid magnitudes ($M_V \lesssim -23.50 \pm 0.10$ mag), although the inclusion of the 13 large-core galaxies has increased the vertical rms scatter around the $R_b - L_V$ relation in the log R_b direction (Δ) by 57%, $\Delta_{\rm normal\text{-}core} \sim 0.30$ dex and $\Delta_{\rm full\_sample} \sim 0.47$ dex (see Table 6). For reference, the slopes of the R_b–L_V relations published by Faber et al. (1997), Laine et al. (2003), de Ruiter et al. (2005), Lauer et al. (2007a), and Rusli et al. (2013) are 1.15, 0.72, 1.05 ± 0.10, 1.32 ± 0.11, and 1.28 ± 0.18.

Finally, in Figures 5, 6(a) and (b) we investigate whether there is an offset or break in the R_b–M_{BH} relation due to normal-core versus large-core spheroids. Of the full sample, 11/44 (three large-core and eight normal-core) galaxies have SMBH mass determined dynamically from stellar or gas kinematic measurements (e.g., Ferrarese & Ford 2005; see Table 5 and Dullo & Graham 2014, their Table 4). We refer to such SMBH masses as "direct" SMBH masses. The OLS bisector finds a remarkably tight R_b-$M_{BH,direct}$ relation for these 11 galaxies ($R_b \propto M_{BH,direct}^{0.83\pm0.10}$, $r \sim 0.92$ and $\Delta \sim 0.24$ dex, see Figure 5). Although we only have 11 galaxies with direct SMBH masses, the R_b–$M_{BH,direct}$ relation found here is in excellent agreement with the core-Sérsic R_b-$M_{BH,direct}$ relation reported by Thomas et al. (2016, Figure 4) for 20 core-Sérsic galaxies with direct SMBH mass measurements: log (R_b/pc) = (0.85 ± 0.10) log ($M_{BH}/10^{9.30}$) + (2.17 ± 0.45). This strongly suggests that the R_b–$M_{BH,direct}$ relation (Table 6) is well constrained.

However, combining these 11 direct SMBH masses with predicted SMBHs for the remaining 30 galaxies without direct SMBH mass measurements, we find that large-core spheroids are offset systematically from the R_b–$M_{BH,direct}$ relation defined by the galaxy sample with measured M_{BH} (dotted lines) and from the R_b–M_{BH} sequence traced by the normal-core spheroids alone (solid lines, Figures 6(a), (b), and Table 6). The slopes of the R_b–M_{BH} relations for the normal-core spheroids are different from those for the full sample (see Table 6). In Figure 6(a), we used the Graham & Scott (2013, their Table 3) non-barred M_{BH}–σ relation to predict the black hole masses for the remaining 30 galaxies without direct SMBH masses, while in Figure 6(b) the predicted SMBH masses were based on the near-linear Graham & Scott (2013, their Table 3) B-band core-Sérsic M_{BH}–L relation transformed here into the V-band using $B-V = 1.0$ (Fukugita et al. 1995). The offset nature of large-core spheroids at the high-mass end of the R_b–M_{BH} relations (Figures 6(a) and (b)) suggest that either extremely massive galaxies have unusually large break radii or the M_{BH}–σ and core-Sérsic M_{BH}–L relations underestimate SMBH masses in extremely massive galaxies, or both cases are true. However, given the tight R_b–μ_b, $R_b - L_V$ and R_b–$M_{BH,direct}$ relations (Figures 3–5), the observed offsets are

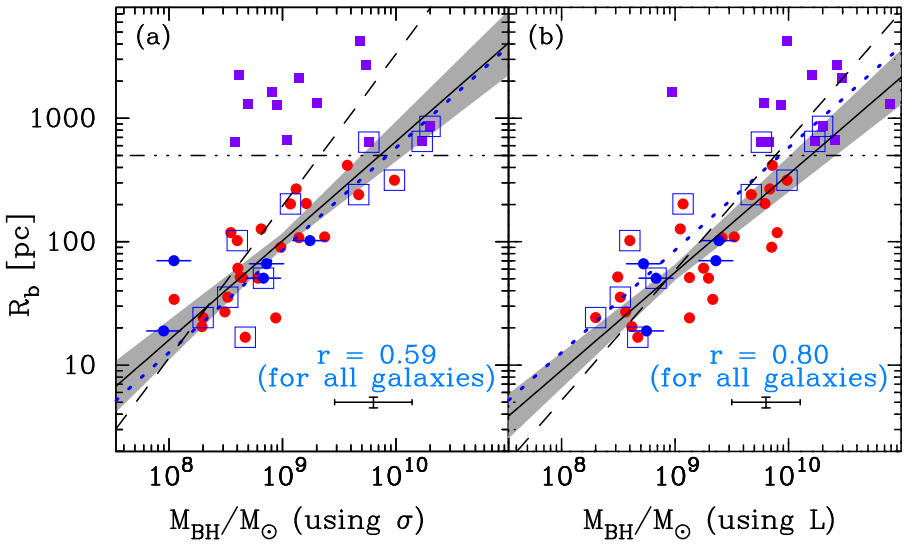

Figure 6. Similar to Figures 4 and 5, but shown here are correlations between the core-Sérsic model break radius, R_b, (Table 3 and Dullo & Graham 2014, their Table 2) and SMBH mass, M_{BH}, (Table 5 and Dullo & Graham 2014, their Table 4). The dotted line is our best OLS fit to the 11 galaxies with dynamically determined SMBH masses (enclosed in boxes, see also Figure 5). For the remaining 30 galaxies, the SMBH masses are estimated using the Graham & Scott (2013) non-barred M_{BH}–σ relation (a) and their B-band core-Sérsic M_{BH}–L relation (b).

likely due to underestimated SMBH masses (e.g., McConnell et al. 2011, 2012; Volonteri & Ciotti 2013; Thomas et al. 2016; Mezcua et al. 2018). Indeed, the direct SMBH measurements in three large-core galaxies (NGC 1600, Thomas et al. 2016, NGC 4889, McConnell & Ma 2013 and Holm 15A, Mehrgan et al. 2019) reveal that, relative to the best-fitting M_{BH}–σ relation, these galaxies are offset by 0.7–1 dex toward large M_{BH}.

Also, combining the R_b–L_V relation (Figure 4) with the R_b–$M_{BH,direct}$ (Figure 5) results in a steeper M_{BH}–L relation ($M_{BH} \propto L_V^{1.66\pm0.25}$, see Table 6) than the Graham & Scott (2013) B-band core-Sérsic M_{BH}–L relation ($M_{BH} \propto L_B^{1.35\pm0.30}$), although the slopes of these two relations are consistent within the 1σ uncertainty. Extrapolating the R_b–$M_{BH,direct}$ relation (Figure 5) to high masses, we find that the M_{BH}–L relation is a better predictor of M_{BH} than the M_{BH}–σ relation for BCGs and central dominant galaxies, confirming the finding by other authors (Bernardi et al. 2007; Lauer et al. 2007a; McConnell et al. 2011, 2012; Volonteri & Ciotti 2013; Mezcua et al. 2018; Phipps et al. 2019).

4.2. Global Structural Relations for Core-Sérsic Galaxies

In a continued endeavor to determine if the scaling relations for normal-core spheroids continue to the large-core spheroids, here we investigate global structural relations involving M_V, the effective (half-light) radius (R_e), and the Sérsic index (n) for our full sample of 41 core-Sérsic spheroids.

4.2.1. σ–L_V

In Figure 7, we show the σ–L_V relation (Faber & Jackson 1976) relation for core-Sérsic spheroids. The OLS bisector yields $\sigma \propto L_V^{1/(5.00\pm0.60)}$ for the 41 core-Sérsic spheroids, compared to the well-known (Faber & Jackson 1976) relation ($\sigma \propto L^{1/4}$). It has been shown that bright core-Sérsic galaxies follow a shallow σ–L relation $\sigma \propto L^{1/(4-8)}$ (e.g., Malumuth & Kirshner 1981; Lauer et al. 2007a; Kormendy & Bender 2013; Sahu et al. 2019), whereas Sérsic galaxies with low luminosities ($M_V \gtrsim -21.5$ mag) define a steeper relation $\sigma \propto L^{1/2}$ (e.g., Held et al. 1992; Matković & Guzmán 2005), see Figure 7. We have identified here a previously unreported substructure in the σ–L_V relation for core-Sérsic spheroids. This relation seems to have a break at $M_V \sim -23.50 \pm 0.10$ mag[8] (Figure 7). At magnitudes brighter than this transition M_V value, the relation flattens and exhibits larger scatter, which may suggest a breakdown. The slope of our σ–L relation for the full sample ($1/(5.00 \pm 0.63)$) is shallower than that found for the normal-core spheroids alone ($1/(3.50 \pm 0.61)$). In Figure 7, we also show Sérsic and core-Sérsic galaxies from Lauer et al. (2007a) to better demonstrate the breaks in the σ–L_V relation but these data points (Lauer et al. 2007a) are not included in the least-squares fits. The σ–L_V relation for Sérsic, normal-core and large-core core-Sérsic galaxies will be investigated in a forthcoming paper.

Our finding is consistent with the notion that major, dry mergers add the stellar mass, black hole mass and sizes in equal proportion while increasing the velocity dispersion only slightly (see also Section 4.2.2). In general, the velocity dispersion for local galaxies does not exceed $\sigma \sim 400$ km s^{-1} (Sheth et al. 2003; Bernardi et al. 2007; Lauer et al. 2007a). As such, the luminosity of large-core galaxies, which are thought to have undergone multiple successive dry mergers, would be unusually bright for the galaxies' σ, compared to the normal-core galaxies. We agree with Bernardi et al. (2007) who found that BCGs follow a shallower σ–L relation than most (other) early-type galaxies (see also Oegerle & Hoessel 1991; Boylan-Kolchin et al. 2006). In contrast, Lauer et al. (2007a, their Equation (7)) and Kormendy & Bender (2013) advocated for a single power-law relation for BCGs and other bright ellipticals with $M_V \lesssim -20.5$ mag. However, the break in the σ–L relation near $M_V \sim -23.50 \pm 0.10$ can easily be seen in Figure 7 and Kormendy & Bender (2013, their Figures 1 and 2). In fact, Kormendy & Bender (2013) wrote that their core and coreless galaxies overlap over the luminosity range -20.50 mag $> M_V > -22.85$ mag. As such, their shallow core-Sérsic σ–L_V

[8] Assuming an old stellar population of $M/L_V = 5.6$, $M_V \sim -23.50 \pm 0.10$ mag yields a stellar mass of $M_* \sim 1.2 \times 10^{12} M_\odot$ for $M_{V,Sun} = 4.83$ mag.

Table 5
Large-core Galaxy Data

Galaxy	*HST* Filter	M/L	log $(M_*/M_\odot)$ (Spheroid)	log $(M_*/M_\odot)$ (Halo/Sérsic comp)	log $(L_{\rm def}/L_\odot)$	log $(M_{\rm def}/M_\odot)$	log $(M_{\rm BH}/M_\odot)$ (σ-based)	log $(M_{\rm BH}/M_\odot)$ (L-based)	log $(M_{\rm BH}/M_\odot)$ ($R_{\rm b}$-based)	$M_{\rm def}/M_{\rm BH}$ (σ-based/L-based/$R_{\rm b}$-based)
(1)	(2)	(3)	(4)	(5)	(6)	(7)	(8)	(9)	(10)	(11)
NGC 1600	F160W [N]	1.60	12.18	10.73	10.49	10.67	$10.23^{+0.04}_{-0.04}$[d1]	$10.23^{+0.04}_{-0.04}$[d1]	$10.23^{+0.04}_{-0.04}$[d1]	2.8/2.8/2.8
NGC 4486	F814W [A]	3.20	12.12	⋯	9.96	10.46	$9.76^{+0.03}_{-0.03}$[d2]	$9.76^{+0.03}_{-0.03}$[d2]	$9.76^{+0.03}_{-0.03}$[d2]	5.1/5.1/5.1
NGC 4874	F606W [W]	3.80	11.32	12.31/11.56	10.23	10.81	$8.91^{+0.42}_{-0.42}$	$8.98^{+0.34}_{-0.34}$	$10.54^{+0.45}_{-0.45}$	79.8/67.6/1.9
NGC 4889	F606W [W]	3.80	12.71	⋯	10.39	10.97	$10.30^{+0.25}_{-0.62}$[d3]	$10.3^{+0.25}_{-0.62}$[d3]	$10.3^{+0.25}_{-0.62}$[d3]	4.7/4.7/4.7
NGC 6166	F814W [A]	3.20	12.53	11.81/8.60	10.71	11.21	$9.14^{+0.43}_{-0.43}$	$10.47^{+0.47}_{-0.47}$	$10.68^{+0.46}_{-0.46}$	117.3/5.5/3.4
MS0735-BCG	F850LP [A]	3.00	12.38	12.67	10.33	10.81	$8.61^{+0.41}_{-0.41}$	$10.20^{+0.43}_{-0.43}$	$10.71^{+0.46}_{-0.46}$	157.0/4.1/1.3
A0119-BCG	F814W [W]	3.20	12.49	11.97	9.66	10.17	$9.04^{+0.43}_{-0.43}$	$10.41^{+0.46}_{-0.46}$	$10.08^{+0.42}_{-0.42}$	13.5/0.6/1.2
A2147-BCG	F814W [W]	3.20	12.13	11.87	10.23	10.74	$8.95^{+0.42}_{-0.42}$	$9.93^{+0.40}_{-0.40}$	$10.42^{+0.44}_{-0.44}$	61.2/6.4/2.1
A2261-BCG	F850LP [A]	3.00	12.61	12.86	10.17	10.65	$9.73^{+0.48}_{-0.48}$	$10.43^{+0.48}_{-0.48}$	$10.81^{+0.45}_{-0.45}$	8.2/1.7/0.7
A3558-BCG	F814W [A]	3.20	12.84	⋯	10.13	10.63	$8.70^{+0.41}_{-0.41}$	$10.89^{+0.54}_{-0.54}$	$10.43^{+0.44}_{-0.44}$	85.7/0.6/1.7
A3562-BCG	F814W [W]	3.20	12.06	12.23	9.62	10.12	$8.59^{+0.41}_{-0.41}$	$9.83^{+0.39}_{-0.39}$	$10.05^{+0.42}_{-0.42}$	34.6/2.0/1.2
A3571- BCG	F814W [A]	3.20	12.04	13.78/11.81	10.25	10.76	$9.31^{+0.44}_{-0.44}$	$9.79^{+0.39}_{-0.39}$	$10.44^{+0.43}_{-0.43}$	28.0/9.3/2.1

Note. Col. (1) galaxy name. Col. (2) *HST* filters and instruments (NICMOCS, N; ACS, A and WFPC2, W). Col. (3) stellar mass-to-light (M/L) ratios are obtained from Worthey (1994) assuming a ∼12 Gyr old stellar population. Cols. (4) and (5) stellar mass of the spheroid, halo and any additional Sérsic components. Col. (6) central stellar luminosity deficit in units of solar luminosity. Col. (7) central stellar mass deficit determined using cols. (3) and (6). Cols. (8), (9), and (10) SMBH masses predicted using the Graham & Scott (2013, their Figure 2 and Table 3) "non-barred $M-\sigma$" relation, their B-band core-Sérsic $M_{\rm BH}$–L relation and the "(direct SMBH)-based $R_{\rm b}$–$M_{\rm BH}$" relation, see the text for details. For three galaxies, we use direct SMBH mass measurements obtained from three different sources and adjusted them to our distances: d1 = Thomas et al. (2016); d2 = Gebhardt et al. (2011); d3 = McConnell et al. (2011). We assume a 10% uncertainty on σ to estimate the error on the predicted SMBH mass. Col. (11) ratios between mass deficit (col. 7) and black hole masses (cols. 8, 9, and 10), $M_{\rm def}/M_{\rm BH}$.

Table 6
Scaling Relations for Core-Sérsic Galaxies

Relation	OLS Bisector Fit	Δ
This work (12 galaxies) + Dullo et al. (2017, 1 core-Sérsic galaxy, IC 1101) + Dullo & Graham (2014, 28 core-Sérsic galaxies]		
R_b–μ_b	$\log\left(\frac{R_b}{pc}\right) = (0.38 \pm 0.02)(\mu_b - 17.50) + (2.45 \pm 0.03)$	0.18 dex
R_b–M_V	$\log\left(\frac{R_b}{pc}\right) = (-0.55 \pm 0.05)(M_V + 23.4) + (2.65 \pm 0.09)$	0.47 dex
R_b–M_{BH} (11 direct M_{BH} masses)	$\log\left(\frac{R_b}{pc}\right) = (0.83 \pm 0.10)\ \log\left(\frac{M_{BH}}{10^{9.30} M_\odot}\right) + (2.18 \pm 0.08)$	0.24 dex
R_b–M_{BH} (M–σ derived M_{BH} for 30 galaxies plus 11 direct M_{BH} masses)	$\log\left(\frac{R_b}{pc}\right) = (1.19 \pm 0.14)\ \log\left(\frac{M_{BH}}{10^{9.30} M_\odot}\right) + (2.64 \pm 0.13)$	0.61 dex
R_b–M_{BH} (M–L derived M_{BH} for 30 galaxies plus 11 direct M_{BH} masses)	$\log\left(\frac{R_b}{pc}\right) = (1.05 \pm 0.09)\ \log\left(\frac{M_{BH}}{10^{9.85} M_\odot}\right) + (2.66 \pm 0.09)$	0.44 dex
σ–M_V	$\log(\sigma) = (-0.08 \pm 0.01)(M_V + 23.40) + (2.49 \pm 0.02)$	0.09 dex
M_V–R_e	$M_V = (-2.32 \pm 0.19)\ \log\left(\frac{R_e}{2 \times 10^{4.00}\ pc}\right) + (-23.19 \pm 0.12)$	0.70
M_V–n	$M_V = (-4.13 \pm 1.87)\ \log\left(\frac{n}{5.0}\right) + (-22.70 \pm 0.21)$	1.25
Dullo & Graham (2014, 28 core-Sérsic galaxies)		
R_b–μ_b	$\log\left(\frac{R_b}{pc}\right) = (0.41 \pm 0.04)(\mu_b - 16.00) + (1.86 \pm 0.04)$	0.18 dex
$R_b - M_V$	$\log\left(\frac{R_b}{pc}\right) = (-0.45 \pm 0.05)(M_V + 22) + (1.79 \pm 0.06)$	0.30 dex
R_b–M_{BH} (M–σ derived M_{BH} for 23 galaxies plus eight direct M_{BH} masses)	$\log\left(\frac{R_b}{pc}\right) = (0.80 \pm 0.10)\ \log\left(\frac{M_{BH}}{10^{9} M_\odot}\right) + (2.01 \pm 0.05)$	0.27 dex
R_b–M_{BH} (M–L derived M_{BH} for 23 galaxies plus eight direct M_{BH} masses)	$\log\left(\frac{R_b}{pc}\right) = (0.79 \pm 0.08)\ \log\left(\frac{M_{BH}}{10^{9} M_\odot}\right) + (1.75 \pm 0.06)$	0.27 dex
Relation	**OLS bisector fit**	***r***
Σ_5–R_b (for nine large-core galaxies excluding the large-core, group galaxy[a] and the three distant, $D \gtrsim 360$ Mpc, sample large-core galaxies)	$\log(\Sigma_5) = (1.51 \pm 0.47)\ \log\left(\frac{R_b}{pc}\right) + (0.78 \pm 0.11)$	0.54
Σ_{10}–R_b (for 10 large-core galaxies excluding the three distant, $D \gtrsim 360$ Mpc, sample large-core galaxies)	$\log(\Sigma_{10}) = (1.61 \pm 0.73)\ \log\left(\frac{R_b}{pc}\right) + (1.05 \pm 0.15)$	0.32

Note. Scatter in the vertical direction (Δ). Pearson correlation coefficient (r).
[a] If we include the only sample large-core, group galaxy NGC 1600 (with a low Σ_5 value $\sim$0.31 Mpc^{-2}, see Figures 10 and 14), then for the 10 large-core galaxies, the OLS bisector finds a relation between Σ_5 and R_b with a slope of 2.40 ± 1.03, an intercept of 0.68 ± 0.17 and $r \sim 0.57$.

relation ($\sigma \propto L_V^{1/(8.33\pm1.24)}$) is mainly driven by galaxies with $M_V \lesssim -22.85$ mag.

4.2.2. L_V–R_e *and* L_V–n

In Figures 8(a) and (b), we investigate the behavior of M_V as a function of the effective radius (R_e) and Sérsic index (n), Table 6. As noted by Dullo & Graham (2014), for a given M_V, the spheroids of core-Sérsic lenticular galaxies tend to be compact ($R_e \lesssim 2$ kpc), see also Dullo & Graham (2013), Graham (2013), Graham et al. (2015), de la Rosa et al. (2016). Excluding the five lenticular galaxies in our sample, we find that large-core and normal-core spheroids follow the same tight correlation between L_V and R_e. A symmetrical OLS fit to the 36(=41−5) core spheroids gives a near-linear $L_V - R_e$ relation $R_e \propto L_V^{1.08\pm0.09}$with $r \sim -0.85$; our slope is slightly steeper than the L–R_e relation for BCGs in Bernardi et al. (2007) $R_e \propto L^{0.88}$.

We find a much weaker correlation between M_V and n for our 41 core-Sérsic spheroids. A symmetrical OLS fit finds $L_V \propto n^{1.65\pm0.75}$ with $r \sim -0.30$ (Table 6). Interestingly, however, the M_{BH}–n relation that we derive combining our L_V–n, R_b–L_V and R_b–$M_{BH,direct}$ relations for the full sample ($M_{BH} \propto n^{2.75\pm1.31}$) has a slope that is consistent with those of the relations in Graham & Driver (2007, slope $\sim2.68 \pm 0.40$) and Davis et al. (2019, slope $\sim2.69 \pm 0.33$).

5. Discussion

5.1. Central Stellar Mass Deficit

The central stellar mass deficits in core-Sérsic spheroids (M_{def}) are useful to explain if the large cores of BCGs and central dominant galaxies reflect the actions of overmassive SMBHs or intense core scouring via large amount of galactic merging or a combination of both. As mentioned in the introduction, the favored mechanism for the creation of central stellar mass deficits is the three-body encounters of the core stars with the inspiraling binary SMBHs that form from dry major mergers (Begelman et al. 1980; Ebisuzaki et al. 1991; Faber et al. 1997; Milosavljević & Merritt 2001; Milosavljević et al. 2002). Using of N-body simulations, Merritt (2006) first revealed that the accumulated stellar mass deficit that is

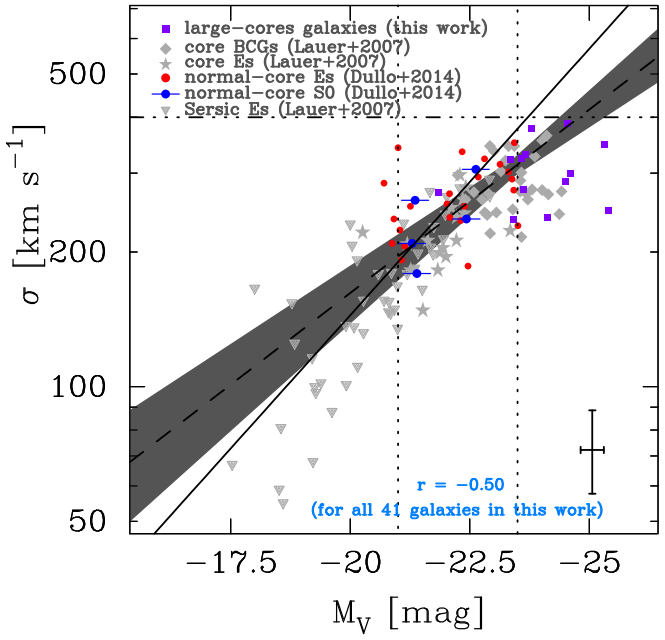

Figure 7. Similar to Figure 4, but showing here the correlation between σ and M_V (Faber & Jackson 1976). The vertical dotted lines indicate the $M_V = -21.0$ mag and $M_V = -23.50$ mag demarcations, corresponding to the Sérsic vs. core-Sérsic and normal-core vs. large-core divides, respectively. The horizontal dashed-dotted line indicates the velocity dispersion function cutoff for local galaxies of $\sigma = 400$ km s^{-1} (e.g., Sheth et al. 2003; Bernardi et al. 2007; Lauer et al. 2007a). The Sérsic and core-Sérsic galaxies from Lauer et al. (2007a), shown here to better reveal the breaks in the σ–L relation, are not included in the least-squares fits.

generated by binary SMBHs after $\mathcal{N}$ numbers of successive dry major mergers scales as $M_{\rm def} \approx 0.5\mathcal{N}M_{\rm BH}$, where $M_{\rm BH}$ is the total sum of the masses of the binary SMBHs.

In order to derive the central stellar mass deficits for the large-core galaxies, we follow the same prescription in Dullo & Graham (2014), Dullo et al. (2017, 2018). The central stellar luminosity deficit ($L_{\rm def}$) is computed as the difference in luminosity between inwardly extrapolated outer Sérsic profile of the complete core-Sérsic model fit to the spheroid (Equation (1)) and the core-Sérsic model itself (Equation (2)). For each galaxy, this luminosity deficit is converted into $M_{\rm def}$ using the stellar mass-to-light ratios (M/L) given in Table 5. We measure stellar mass deficits for the large-core galaxies that are $M_{\rm def} \gtrsim 10^{10} M_\odot$, larger than those for normal-core galaxies $M_{\rm def} \lesssim 10^{10} M_\odot$ except for NGC 5419. The BCG, NGC 5419, of the poor cluster AS753 is a normal-core galaxy with $R_{\rm b} \sim 416$ pc and $M_{\rm def} \sim 2.3 \times 10^{10} M_\odot$ (Dullo & Graham 2014).

Figure 9 shows the mass deficits as a function of directly measured or predicted SMBH masses. For the 11 core-Sérsic galaxies in the sample with directly measured $M_{\rm BH}$ we find $M_{\rm def} \sim 0.5 - 5\, M_{\rm BH}$, consistent with spheroid formation via a reasonably large number of dry major merger events (1−10, Merritt 2006). This figure is consistent with $M_{\rm def}/M_{\rm BH}$ ratio we find for the normal-core galaxies without direct $M_{\rm BH}$; using SMBH masses predicted based on the $M_{\rm BH}$–σ relation (Dullo & Graham 2014, their Table 4) gives $M_{\rm def} \sim 0.5 - 4\, M_{{\rm BH},\sigma\text{-based}}$. Our findings also agree with previous work that derived $M_{\rm def} \sim 0.5$–$4\, M_{\rm BH}$ for normal-core galaxies using similar methods (e.g., Graham 2004; Ferrarese et al. 2006; Dullo & Graham 2013, 2014; Rusli et al. 2013; Dullo et al. 2018) and with Hopkins & Hernquist (2010) who calculated $M_{\rm def}$ via a model-independent analysis of the light profiles, rather than determining the difference in luminosity between a Sérsic fit and a core-Sérsic fit as done here, finding $M_{\rm def} \sim 2\, M_{\rm BH}$. Our results can also be compared with studies that estimated the merger rates for massive galaxies from observations of close galaxy pairs, finding that massive galaxies have undergone 0.5–4 major mergers since $z \sim 3$ (e.g., Bell et al. 2006; Conselice 2007; Liu et al. 2009; Bluck et al. 2012; Edwards & Patton 2012; Lidman et al. 2013; Man et al. 2016; Mundy et al. 2017; Duncan et al. 2019).

Of particular importance here is that the large-core galaxies without direct $M_{\rm BH}$ have predicted SMBH masses ($M_{{\rm BH},\sigma\text{-based}}$ and $M_{{\rm BH},L\text{-based}}$) that are undermassive for their stellar mass deficits (Figure 9 and Table 5). This echos the offset nature of the predicted SMBH masses of large-core spheroids shown in Figure 6. We find $M_{\rm def} \sim (10 - 160)\, M_{{\rm BH},\sigma\text{-based}}$ and $M_{\rm def} \sim (2 - 70)\, M_{{\rm BH},L\text{-based}}$. These figures correspond to unrealistically high number of major dry mergers ($\mathcal{N} \sim 5 - 320$) for the bulk (∼70%) of the large-core spheroids. We argue that the excessive merger rates have arisen because the $M_{\rm BH}$–σ and $M_{\rm BH}$–L relations significantly underestimate the SMBH masses for large-core galaxies (see Section 4.1). On the other hand, the $R_{\rm b}$–$M_{\rm BH,direct}$ relation for the core-Sérsic spheroids (Figure 5) is such that the predicted SMBH masses for the large-core spheroids based on $R_{\rm b}$ are typically a factor of 1.7–4.5 (and 10–43), i.e., ∼0.6–1.7σ (and ∼3.7–15.6σ), larger than expectations from the spheroid L (and σ), Table 5. If we use these $R_{\rm b}$ based SMBH masses then the derived number of major, dry mergers for large-core galaxies would be $\mathcal{N} \sim 2 - 7$ (Table 5), in good agreement with observations and theoretical expectations in a hierarchical universe.

It is worthwhile noting that enhanced core scouring can occur due to a gravitational radiation-recoiled SMBH[9] (e.g., Redmount & Rees 1989; Boylan-Kolchin et al. 2004; Merritt et al. 2004; Gualandris & Merritt 2008). While substantial SMBH recoiling events would lower the inferred merger rates by a few, this process does not account for the unrealistically high values of $\mathcal{N}$ quoted above. We also note the binary SMBH core scouring scenario assumes that the SMBH binaries coalesce in most merged galaxies via the emission of gravitational wave. The alternative scenario is multiple SMBH systems form (e.g., Liu et al. 2019), generating large stellar mass deficits due to the gravitational sling-shot ejection of the SMBHs (Kulkarni & Loeb 2012). This process would lead to a smaller SMBH mass, at odds with the tight $R_{\rm b}$–$M_{\rm BH}$ correlation for core-Sérsic spheroids (Figure 5). Furthermore, in Section 5.2, we also show that the excessive merger rates cannot be explained by the galaxy environment.

5.2. Impact of Environment on the Break Radius and Galaxy Merger Rate

Given the rarity of large-core galaxies, it is of interest to explore the impact of the environment on their break radii and major merger histories. All of the large-core galaxies in our sample except for three (NGC 1600, NGC 4486, and NGC 4874) are classified as BCGs (Section 2.2). NGC 1600 is the brightest member of the poor NGC 1600 group, whereas NGC

[9] Interested readers are referred to Section 5.4 of Dullo & Graham (2014) and Section 6.1 of Dullo & Graham (2013) for further discussions on alternative mechanisms for the formation of enhanced depleted cores.

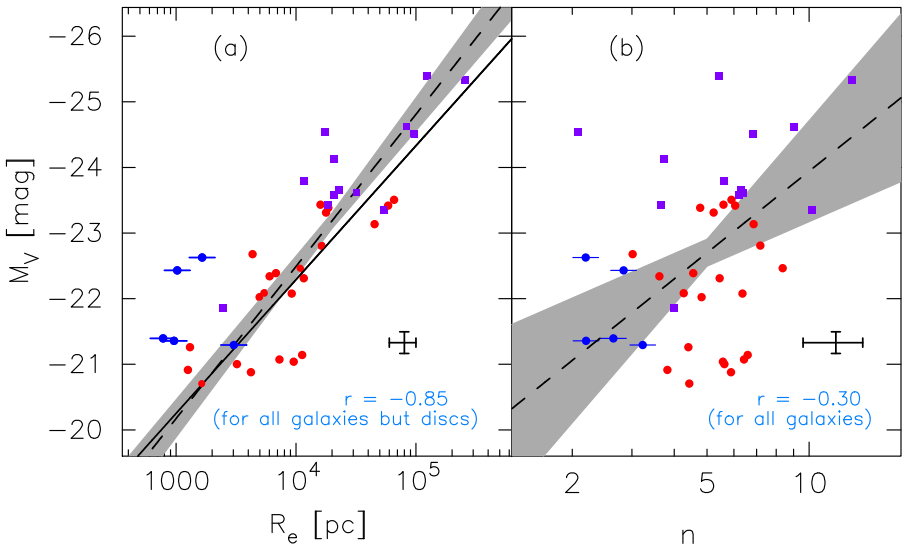

Figure 8. Similar to Figure 4, but shown here are correlations between V-band spheroid absolute magnitude and effective radius R_e (a) and Sérsic index n (b). For the L_V–R_e relation (a), the dashed line is a symmetric least-squares fit to the 36(=41–5) core-Sérsic galaxies after excluding the 5 S0 galaxies in the sample, while the solid line is a symmetric least-squares fit to the 23 normal-core elliptical galaxies (Dullo & Graham 2014). For the L_V–n relation (b), we show a symmetric least-squares fit to full sample of 41 core-Sérsic galaxies (dashed line).

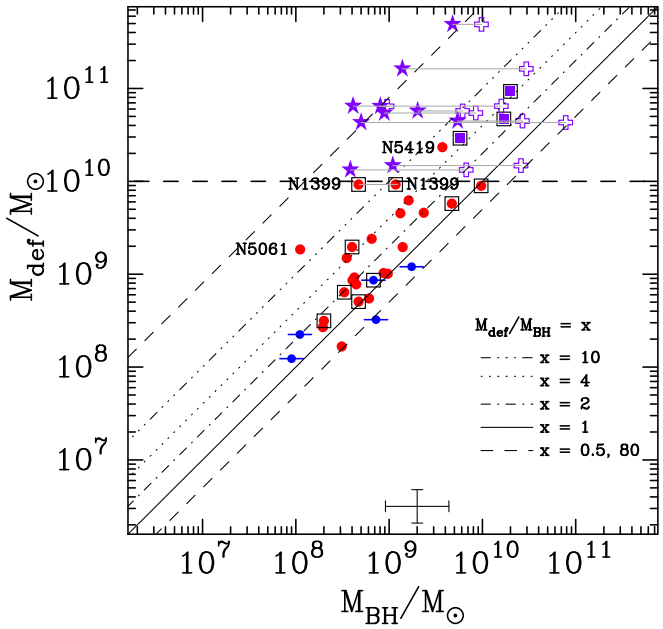

Figure 9. Central mass deficit ($M_{\rm def}$) plotted as a function of black hole mass ($M_{\rm BH}$). For 11 galaxies enclosed in boxes, we used their dynamically determined SMBH masses (Table 5 and Dullo & Graham 2014, their Table 4). For NGC 1399, we plot two direct SMBH mass measurements. For the remaining 30 galaxies, the SMBH masses were estimated using the M–σ (filled disks, filled circles and filled stars) or M–L relations (open crosses). All 13 large-core galaxies shown in purple (filled boxes, filled stars and open crosses) have $M_{\rm def} \gtrsim 10^{10} M_\odot$, whereas the normal-core galaxies (filled red circles and blue disks) typically have $M_{\rm def} \lesssim 10^{10} M_\odot$. A representative error bar is shown at the bottom of the panel.

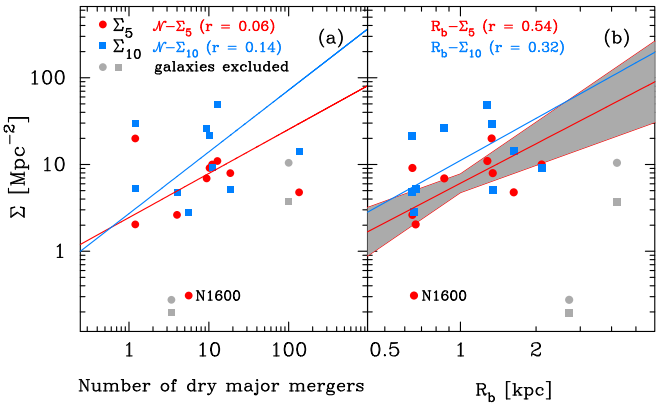

Figure 10. Comparison of environmental measures (Σ_5 and Σ_{10}) with the number of major dry mergers $\mathcal{N}(\approx 2M_{\rm def}/M_{\rm BH}$, Merritt 2006) (a) and break radius $R_{\rm b}$ (b) for our nine large-core galaxies, excluding two of the three most distant sample galaxies in our sample with $D \gtrsim 360$ Mpc (A2261-BCG and IC 1101, gray points) and the BCG 4C +74.13 with no robust data for its nearest neighbors in NED (Table 1). We use $\mathcal{N}$ derived using $M_{\rm BH,L\text{-}based}$ or direct $M_{\rm BH}$ when available. Σ_5, which is based on the five nearest neighboring galaxies with $M_B \lesssim -19.5$ mag, is less affected by distance than Σ_{10}, calculated using the 10 nearest neighbors with $M_B \lesssim -18$ mag. Overall, the galaxy merger rate exhibits no significant dependence the environment estimates (see the text). On the other hand, large-core galaxies in high-density regions tend to exhibit larger depleted cores than those in relatively low-density environments.

4486 and NGC 4874 are the second BCGs sitting at the center of their host clusters.

Following Cappellari et al. (2011, their Section 3.1), we make use of two parameters (Σ_5 and Σ_{10}) to obtain an estimate of the galaxy environment. The surface density Σ_{10} is defined as $N_{\rm gal}/(\pi R_{10}^2)$, where R_{10} is the radius, centered on a large-core galaxy, that encloses the 10 nearest neighbors with $M_B \lesssim -18.0$ mag and the relative recession velocity of the galaxies $|V_{\rm hel,large\text{-}core} - V_{\rm hel,neighbour}| < 300$ km s^{-1}. Similarly, $\Sigma_5 = N_{\rm gal}/(\pi R_5^2)$, where R_5 is the radius centered on a large-core galaxy enclosing the five nearest neighbors with $M_B \lesssim -19.5$ mag and $|V_{\rm hel,large\text{-}core} - V_{\rm hel,neighbour}| < 300$ km s^{-1}. The nearest neighbor identification, recession velocities ($V_{\rm hel}$) are based on NED, while the B-band absolute galaxy magnitudes are from Hyperleda. We excluded the large-core galaxy 4C +74.13 with no robust data for its nearest neighbors in NED. The caveat here is that galaxies with $M_B \gtrsim -19.5$ mag may be too faint for detection at the distances of 4C +74.13 ($D \sim 925$ Mpc), A2261-BCG ($D \sim 959$ Mpc) and IC 1101 ($D \sim 363$ Mpc), see

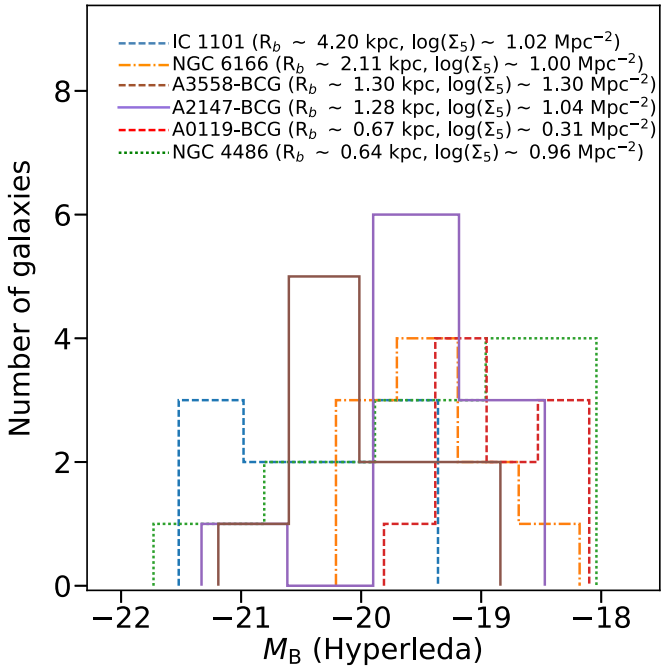

Figure 11. Histograms of absolute B-band galaxy magnitudes (M_B, Hyperleda) of the 10 nearest neighbors (with $M_B \lesssim -18$ mag) for six large-core galaxies (NGC 4486, NGC 6166, A0119-BCG, A2147-BCG, A3558-BCG, and IC 1101), Table 1. These six galaxies have representative break radii for the large-core galaxy population, allowing us to explore the trend between the break radii of large-core galaxies (R_b) and the luminosities of their 10 nearest neighbors. Large-core galaxies with brighter neighbors appear to have larger depleted cores.

Figures 10, 11 and Appendix B. Therefore, we caution that A2261-BCG and IC 1101 can be biased toward having brighter nearest neighbors and low Σ_{10}, compared to the other large-core galaxies with $D \lesssim 213$ Mpc (see Appendix B).

Figure 10 shows the trends between environmental measures (Σ_5 and Σ_{10}) and (a) number of major dry mergers $\mathcal{N}$ and (b) break radius R_b for the 12 large-core galaxies in our sample (see also Appendix B). The values of $\mathcal{N}$ were derived using L-based SMBH masses ($M_{BH,L\text{-based}}$) or direct M_{BH} when available (see Table 5). Excluding A2261-BCG and IC 1101, we find significant correlations between R_b and Σ_5 and Σ_{10}, in the sense that large-core galaxies in high-density regions tend to exhibit larger R_b than those in relatively low-density environments (Table 6). These correlations also reveal that more massive SMBHs are hosted by large-core galaxies that reside in denser environments. The Pearson correlation coefficients for the Σ_5–R_b and Σ_{10}–R_b relations are $r \sim 0.54$–0.57 and $r \sim 0.32$, respectively.

We do not witness a correlation between the number of dry major mergers $\mathcal{N}$ and the environment estimates Σ_5 and Σ_{10} ($r \sim 0.06$–0.14). Accordingly, the excessive amount of major mergers that we obtained for a couple of large-core galaxies ($\mathcal{N} \gtrsim 5 - 320$, Section 5.1 and Figure 9) cannot be readily explained by their local projected environmental densities. Instead, the L-based SMBH masses—which we used to calculate the merger rates ($\mathcal{N} \approx 2M_{def}/M_{BH}$, Merritt 2006) for the bulk (7/10) of the galaxies in Figure 10—may explain the high $\mathcal{N}$ values as well as the poor Σ-$\mathcal{N}$ correlation, since $M_{BH,L\text{-based}}$ appear to be undermassive for the break radii (R_b) and mass deficits (M_{def}) of large-core galaxies (Figures 6 and 9).

In Figure 11, we show histograms of absolute B-band galaxy magnitudes (M_B) of the 10 nearest neighbors with $M_B \lesssim -18$ mag for six large-core galaxies (NGC 4486, NGC 6166, A0119-BCG, A2147-BCG, A3558-BCG, and IC 1101). These six large-core galaxies are selected to have representative break radii for the large-core galaxy population. We cannot presently reach a firm conclusion, but there is a hint that large-core galaxies with larger break radii and high Σ_5 have brighter companions (see also Appendix B). This reinforces the idea that the most massive galaxies experience a higher proportion of mergers between massive spheroidal systems.

5.3. Formation of Core-Sérsic Galaxies: "Large-core" versus "Normal-core" Galaxies

We postulate that both "large-core" and "normal-core" core-Sérsic spheroids are built through a reasonably large number of successive dry major mergers ($\mathcal{N} \sim 1 - 10$) involving SMBHs (e.g., Faber et al. 1997; Kormendy 1999; Laine et al. 2003; Trujillo et al. 2004; Bell et al. 2006; Ferrarese et al. 2006; Lauer et al. 2007a; Kormendy et al. 2009; Liu et al. 2009; Bernardi et al. 2011; Dullo & Graham 2013, 2014, 2015; Rusli et al. 2013; Dullo et al. 2017, 2018). In the previous sections, we have shown that "large-core" spheroids of BCGs and central dominant galaxies with $R_b \gtrsim 0.5$ kpc, $M_V \lesssim -23.50 \pm 0.1$ mag, $M_{def} \gtrsim 10^{10} M_\odot$ are extremely massive (i.e., $M_* \gtrsim 10^{12} M_\odot$). The same μ_b–R_b, R_b–L_V, L_V–R_e, and L_V–n relations defined by the "normal-core" core-Sérsic spheroids with $R_b \lesssim 0.5$ kpc, -20.70 mag $\gtrsim M_V \gtrsim -23.60$ mag, $M_{def} \lesssim 10^{10} M_\odot$ and stellar masses $M_* \sim 8 \times 10^{10}$–$10^{12} M_\odot$ hold up at higher masses for the large-core spheroids. This is also the case for the R_b–M_{BH} relation when using directly measured SMBH masses.

The bulk (~77%) of our large-core galaxies are BCGs, which is unsurprising as BCGs are predicted to experience a more intense merging and accretion events than galaxies with relatively low luminosities. Our findings hint that large-core spheroids are more likely to undergo a higher proportion of dry major mergers than the normal-core spheroids. Although we only have three large-core spheroids with measured M_{BH}, we find $\mathcal{N} \sim 6 - 10$ for these spheroids, whereas the bulk (6/8) of our normal-core spheroids with measured M_{BH} have $\mathcal{N} \sim 2 - 4$, see Figure 9. This is in line with the analytic and semi-analytic study by Volonteri & Ciotti (2013); however, see Savorgnan & Graham (2015). Krajnović et al. (2018) also found that about half of the most massive galaxies ($M_* \gtrsim 10^{12} M_\odot$) exhibit prolate-like rotation, consistent with these galaxies being products of dry major mergers. The depleted cores and stellar mass deficits in large-core spheroids likely reflect the cumulative effect of multiple dry mergers and the ensuing excavation of inner stars from the core by coalescing, overmassive black hole binaries with a final mass $M_{BH} \gtrsim 10^{10} M_\odot$ (Sections 4.1 and 5.1), typically a factor of 1.7−4.5 (and 10−43) larger than the SMBH masses estimated using the spheroids' L (and σ). In passing, we note that Mezcua et al. (2018, see also Hlavacek-Larrondo et al. 2012) wrote that 40% of their sample of 72 BCGs at redshift of $z \sim 0.006$–0.300 must have $M_{BH} \gtrsim 10^{10} M_\odot$ to lie on the fundamental plane of black hole accretion. The analytic arguments by King & Nealon (2019) predict present-day galaxies with overmassive black holes that lie above the M_{BH}–σ relation may be

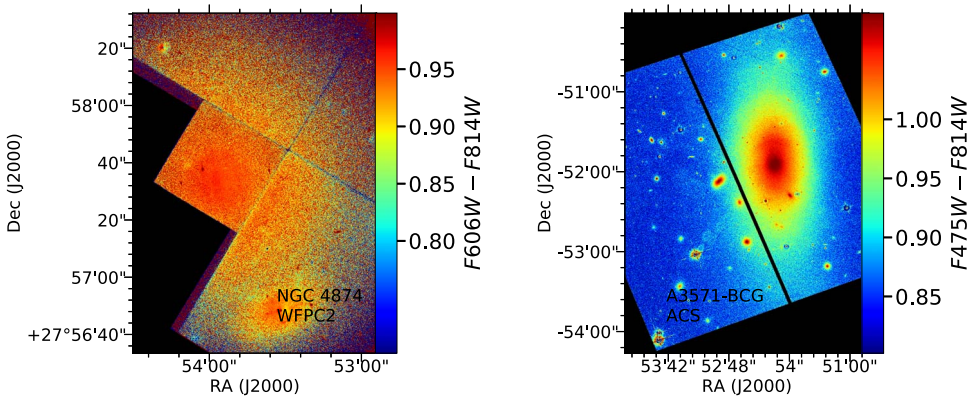

Figure 12. *HST* WFPC2 F606W − F814W and *HST* ACS F475W − F814W color maps for the two large-core galaxies in our sample with intermediate-scale components (NGC 4874 and A3571-BCG). The maps reveal that the galaxies turn bluer with increasing radius. North is up and east is to the left.

descendants of the compact blue nuggets formed at $z \gtrsim 6$, suggesting an evolutionary link between the high-redshift blue nuggets and large-core galaxies.

The higher prevalence of dry mergers associated with large-core spheroids can explain the break that we identified for the first time in the core-Sérsic σ–L_V relation occurring at $M_V \sim -23.50 \pm 0.10$ mag, not to be confused with the change in the slope of the σ–L_V relation due to core-Sérsic versus Sérsic galaxies. The prediction that major, dry mergers add the stellar mass, black hole mass, and sizes in equal proportion while increasing the velocity dispersion only slightly (e.g., Nipoti et al. 2003; Ciotti et al. 2007; Oser et al. 2012; Hilz et al. 2013) would imply that the σ–L_V relation may not hold across the full mass range of core-Sérsic spheroids. We find a flattening of the slope of the σ–L_V relation and larger scatter at the extremely massive end, where the velocity dispersions of the large-core spheroids increase only slightly with L_V, compared to the relatively steep σ–L_V relation for normal-core galaxies (Figure 7).

Turning to the intermediate- and large-scale components, as noted in Section 3.1, of the 13 large-core galaxies in our sample, 10 have low surface brightness outer stellar halos with exponential-like distribution of stars and with physical scales of $R_e \sim$ 10–300 kpc (Appendix A and Dullo et al. 2017, see also Seigar et al. 2007; Pierini et al. 2008; Alamo-Martínez & Blakeslee 2017). The spheroid-to-halo effective radius ratios for the large-core galaxies are $R_{e,spheroid}/R_{e,halo} \sim 0.05$–1 (Tables 3 and 4). Three out of these 10 large-core galaxies (NGC 4874, A3571 and IC 1101) also exhibit intermediate-scale components. The color maps for these three galaxies become gradually bluer toward larger radii (see Figure 12 and Dullo et al. 2017, their Figure 6). The color maps of NGC 4874 and A3571 (Figure 12) were created adopting the same prescription described in Dullo et al. (2017, their Section 3.3). Coupled with our decompositions, these color maps suggest different origins for the inner, red spheroid with a high concentration of old stars and the intermediate- and large-scale components with relatively bluer colors. We find that, when present, the fractional contributions of the outer halos and intermediate-scale components are typically ∼15%–60% and ∼20% of the total (i.e., spheroid + intermediate-component + halo) flux, respectively (similar results have been previously reported by, e.g., Gonzalez et al. 2005; Seigar et al. 2007; Oser et al. 2010; Jiménez-Teja & Dupke 2016).

It appears plausible that the natural assembly pathways for the intermediate-scale and outer halo components of large-core galaxies are significant accretion of less massive neighbors and the accumulation of stars stripped during galaxy-galaxy encounters occurring at $z < 1$ (e.g., Seigar et al. 2007; Naab et al. 2009; Zolotov et al. 2009; Oser et al. 2010; Donzelli et al. 2011; Hilz et al. 2012, 2013; Johansson et al. 2012; Burke et al. 2015; Cooper et al. 2015; Rodriguez-Gomez et al. 2016; Dullo et al. 2017, 2018; Montes & Trujillo 2018; Pillepich et al. 2018). A small contribution to the intermediate-components and halo lights could come from core stars, which are gravitationally ejected by the SMBH binaries and accumulate at large radii outside of the core or escape from the spheroid at high velocities (e.g., Hills 1988; O'Leary & Loeb 2008; Brown et al. 2012). The masses of these ejected stars (i.e., the stellar mass deficits) in large-core galaxies are typically ∼10%–20% (and ∼1%–3%) of the stellar masses of their intermediate- (and outer halo) components (Table 5). Moreover, the observed trend of outwardly rising ellipticity for the large-core galaxies, except for the only group galaxy in our sample, NGC 1600 (Appendix A) suggests that the halo (and perhaps also the intermediate-scale component) stars at large radii trace the global cluster potential rather than the host spheroid potential (e.g., di Tullio 1979; Porter et al. 1991; Postman & Lauer 1995; Dubinski 1998; Gonzalez et al. 2005; Khosroshahi et al. 2006; West et al. 2017).

6. Conclusions

Motivated by the need to re-investigate the formation and structural scaling relations of massive galaxies over a wide dynamic range in spheroid luminosity and stellar mass, we have extracted composite (*HST* WFPC2, ACS, and NICMOS plus ground-based) major-axis surface brightness and ellipticity profiles for 12 extremely massive core-Sérsic galaxies (nine BCGs, two second brightest cluster galaxies, and one brightest group galaxy) with core sizes $R_b > 0.5$ kpc. We perform careful, multicomponent (halo/intermediate-scale component/spheroid/nucleus) decompositions of these composite light profiles, which typically cover a large radial range $R \gtrsim 100''$. In so doing, we modeled the spheroid with a core-Sérsic profile and, when present, we fit an exponential function to the outer halo, a Sérsic model to the intermediate-scale component, and a Gaussian or a Sérsic profile to the nucleus. This is the first time this has been done for the full sample of 12 galaxies. The

decompositions yield an excellent fit to the light profiles of the galaxies with a median rms scatter of 0.031 mag arcsec^{-2}.

We additionally included the galaxy with largest depleted core detected to date IC 1101 ($R_b \sim 4.2$ kpc) from Dullo et al. (2017) and 28 core-Sérsic early-type galaxies with $R_b < 0.5$ kpc from Dullo & Graham (2014). This resulted in the largest sample of 41 core-Sérsic galaxies studied to date, which consists of 13 "large-core" galaxies having $R_b > 0.5$ kpc and the remaining 28 "normal-core" galaxies have $R_b < 0.5$ kpc. Our principal conclusions are as follows:

(1) We find that large-core spheroids have V-band absolute magnitude $M_V \lesssim -23.50 \pm 0.10$ mag, sizes $R_e \gtrsim$ 10–300 kpc and stellar masses that are typically $M_* \gtrsim 10^{12} M_\odot$, whereas for the relatively less luminous normal-core spheroids (-20.70 mag $\gtrsim M_V \gtrsim -23.60$ mag), $R_e \sim$ 1–50 kpc, and $M_* \sim 8 \times 10^{10}$–$10^{12} M_\odot$. Of the 13 large-core galaxies, seven have $R_b \gtrsim 1.3$ kpc. The depleted cores and stellar mass deficits in large-core spheroids are likely due to the cumulative effect of multiple dry mergers and the ensuing core scouring by coalescing, overmassive SMBH binaries with a final mass $M_{BH} \gtrsim 10^{10} M_\odot$. For such galaxies, an additional mechanism that can contribute to the large cores/stellar mass deficits is oscillatory core passages by a (gravitational radiation)-kicked SMBH.

(2) The detailed multicomponent decompositions of the large-core galaxies reveal the bulk ($\sim$77%) of them exhibit low surface brightness outer stellar halos with exponential-like stellar distribution and physical scales of $R_e \sim$ 10–300 kpc.

(3) We present updated structural parameter relations for our 41 massive galaxies with a large range in galaxy luminosity (Section 4). We find that large-core spheroids follow the same μ_V–R_b, R_b–L_V, L_V–R_e, and L_V–n relations defined by the relatively less massive, normal-core spheroids. The strong correlations between R_b, and the break surface brightness (μ_b) and the spheroid luminosity (L_V) for core-Sérsic galaxies are such that $R_b \propto \mu_b^{0.38\pm0.02}$ and $R_b \propto L_V^{1.38\pm0.13}$. We also find a tight, linear relation between the spheroid's luminosity and size for massive (core-Sérsic) ellipticals and BCGs such that $R_e \propto L_V^{1.08\pm0.09}$.

(4) We find a strong log-linear R_b–M_{BH} relation for 11 sample galaxies with directly determined SMBH masses ($R_b \propto M_{BH}^{0.83\pm0.10}$): three of these 11 galaxies are large-core galaxies.

(5) For normal-core galaxies, the break radius R_b correlates equally well with the directly determined SMBH mass ($M_{BH,direct}$) and the SMBH masses predicted using the M_{BH}–σ and the core-Sérsic M_{BH}–L relations ($M_{BH,\sigma\text{-based}}$ and $M_{BH,L\text{-based}}$, Graham & Scott 2013). In contrast, our large host galaxy luminosity range has revealed significant offsets in the R_b–$M_{BH,\sigma\text{-based}}$ and R_b–$M_{BH,L\text{-based}}$ diagrams at the highest galaxy masses (i.e., $M_* \gtrsim 10^{12} M_\odot$). The offset is more pronounced in the former relation. The SMBH masses of large-core galaxies estimated from the M_{BH}–L relation are roughly an order of magnitude larger than those from the M_{BH}–σ relation. We determined that these offsets arise because the SMBH masses in the most massive galaxies (i.e., $M_* \gtrsim 10^{12} M_\odot$) are high relative to what is expected from their velocity dispersions or bulge luminosities. For such galaxies, we recommend the R_b–$M_{BH,direct}$ relation should be used for determining the SMBH masses.

(6) We have measured central stellar mass deficits in large-core galaxies ($M_{def} \gtrsim 10^{10} M_\odot$), which when compared to $M_{BH,direct}$, $M_{BH,\sigma\text{-based}}$, and $M_{BH,L\text{-based}}$ yield M_{def}/M_{BH} ratios of $\sim$0.5–5, $\sim$10–160, and $\sim$2–70, respectively. While the former ratio translates to a reasonably large merger rate (i.e., $\mathcal{N} \sim$ 1–10), the latter two correspond to unrealistically large number of major dry mergers ($\mathcal{N} \sim$ 5–320) for the bulk ($\sim$70%) of the large-core spheroids. These findings strengthen the conclusions above: the central SMBH mass in large-core galaxies is considerably larger than the expectations from the spheroid σ and L. On the other hand, the predicted SMBH masses for the large-core spheroids based on R_b are of the order of $M_{BH} \gtrsim 10^{10} M_\odot$ (Table 5), and typically a factor of 1.7−4.5 (and 10−43), i.e., $\sim$0.6–1.7σ (and $\sim$3.7–15.6σ), larger than the SMBH masses estimated using the spheroids' L (and σ). Using these R_b-based SMBH masses for the large-core galaxies brings down the merger rate to $\mathcal{N} \sim$ 2–7, which is in good agreement with observations and theoretical expectations.

(7) We find significant correlations between R_b and galaxy environment estimates Σ_5 and Σ_{10}, i.e., $r \sim$0.54–0.57 and $r \sim$0.32, respectively. Large-core galaxies in high-density regions tend to exhibit larger R_b than those in relatively low-density environments. Our findings also reveal that more massive SMBHs are hosted by large-core galaxies that reside in denser environments. In contrast, the galaxy merger rate exhibits no significant dependence on the environment estimates. We therefore rule out the excessive amount of major mergers that we obtained for a couple of large-core galaxies ($\mathcal{N} \sim 5 - 320$) being due to higher local projected environmental densities.

(8) Our results hint that large-core spheroids are more likely to experience a higher proportion of dry major mergers than the normal-core spheroids (see, e.g., Volonteri & Ciotti 2013). Although our sample only contains three large-core spheroids with measured M_{BH}, we find $\mathcal{N} \sim 6 - 10$ for these spheroids, compared to $\mathcal{N} \sim 2 - 4$ for the bulk (6/8) of our normal-core spheroids with measured M_{BH}.

(9) We discover a break in the core-Sérsic σ–L_V relation occurring at $M_V \sim -23.50 \pm 0.10$ mag, not to be confused with the change in the slope of the σ–L_V relation due to core-Sérsic versus Sérsic galaxies. We attribute this to be the result of large-core spheroids undergoing more dry major mergers than the relatively less massive, normal-core spheroids.

Our findings carry significant implications for studies that attempt to predict SMBH masses in the most massive galaxies using their spheroid luminosity (L) or σ. Future high-resolution dynamical SMBH mass measurements by modeling stellar or ionized gas kinematics in galaxies with $M_V \lesssim -23.50 \pm 0.1$ mag and $M_* \gtrsim 10^{12} M_\odot$ are imperative to further study the processes that shaped the growth of the most massive galaxies and their SMBHs.

I thank the referee for the timely report and constructive suggestions that improved the original manuscript. I am grateful to Berta Margalef-Bentabol, Cristina Cabello, and Mario Chamorro-Cazorla for their comments on this work. I acknowledge support from a Spanish postdoctoral fellowship "Ayudas 1265 para la atracción del talento investigador. Modalidad 2: jóvenes investigadores." funded by Comunidad de Madrid under grant No. 2016-T2/TIC-2039. I acknowledge financial support

from the Spanish Ministry of Science, Innovation and Universities (MCIUN) under grant Nos. AYA2016-75808-R and RTI2018-096188-B-I00. This research made use of APLpy, an open-source plotting package for Python (Robitaille & Bressert 2012) and the NASA/IPAC Extragalactic Database (NED), which is operated by the Jet Propulsion Laboratory, California Institute of Technology, under contract with the National Aeronautics and Space Administration. Based on observations made with the NASA/ESA *Hubble Space Telescope*, and obtained from the Hubble Legacy Archive, which is a collaboration between the Space Telescope Science Institute (STScI/NASA), the Space Telescope European Coordinating Facility (ST-ECF/ESA) and the Canadian Astronomy Data Centre (CADC/NRC/CSA). This publication makes use of data products from the Two Micron All Sky Survey, which is a joint project of the University of Massachusetts and the Infrared Processing and Analysis Center/California Institute of Technology, funded by the National Aeronautics and Space Administration and the National Science Foundation.

Appendix A

In Figure 13, we show the multicomponent decomposition of the major-axis surface brightness profiles of the large-core galaxies (Table 1).

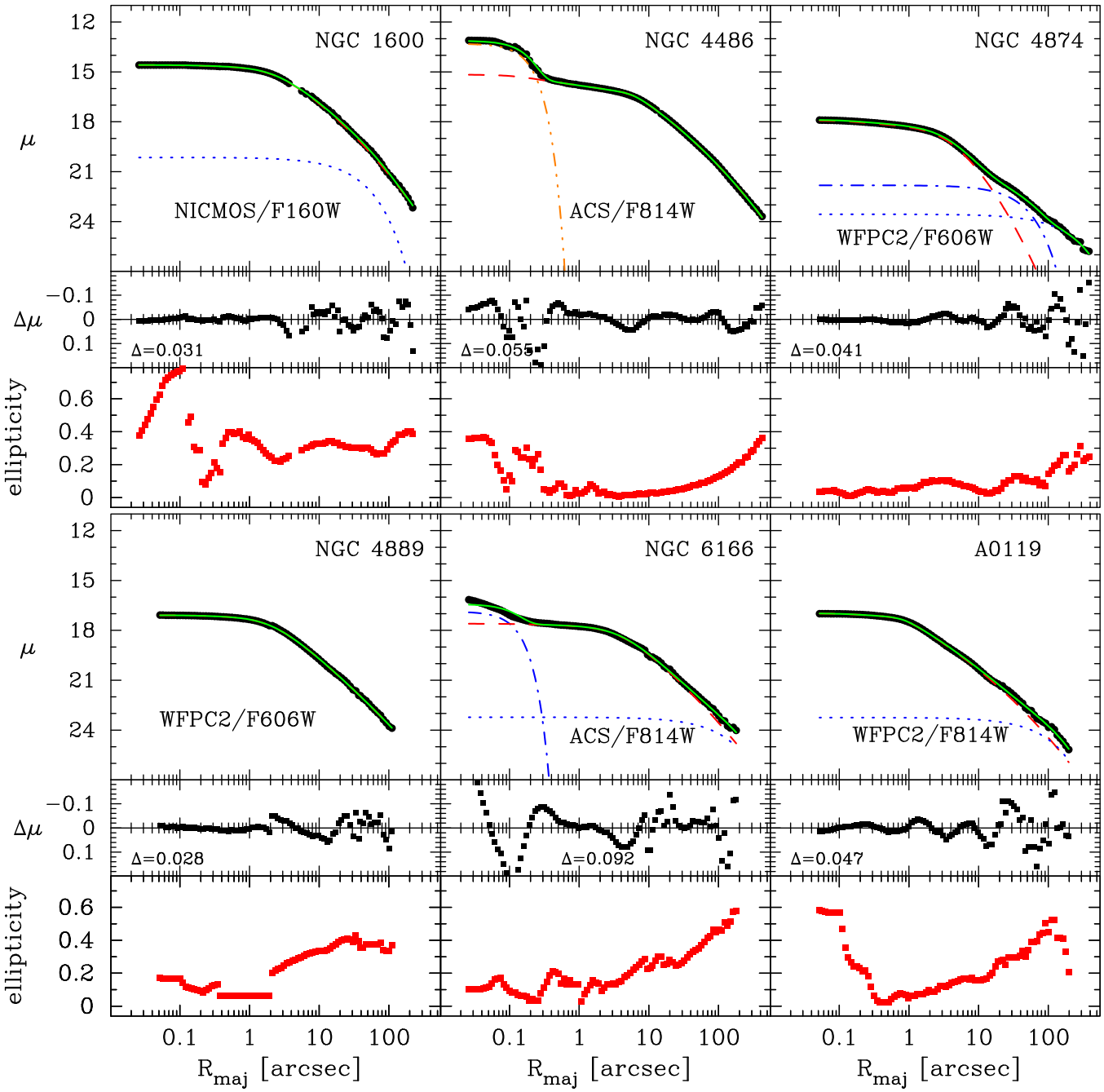

Figure 13. Fits to the major-axis surface brightness profiles of our sample of 12 core-Sérsic galaxies (see Table 1). The red dashed curves indicate the core-Sérsic model, while the blue dotted curves show the outer stellar halo. Additional nuclear light components such as AGN and star clusters were modeled using either a Gaussian (brown, triple dotted–dashed curve) or a Sérsic function (blue dotted–dashed curve). The solid green curves represent the complete fit to the profiles. The fit rms residuals and ellipticity ($\epsilon = 1 - b/a$) are given in the lower panels.

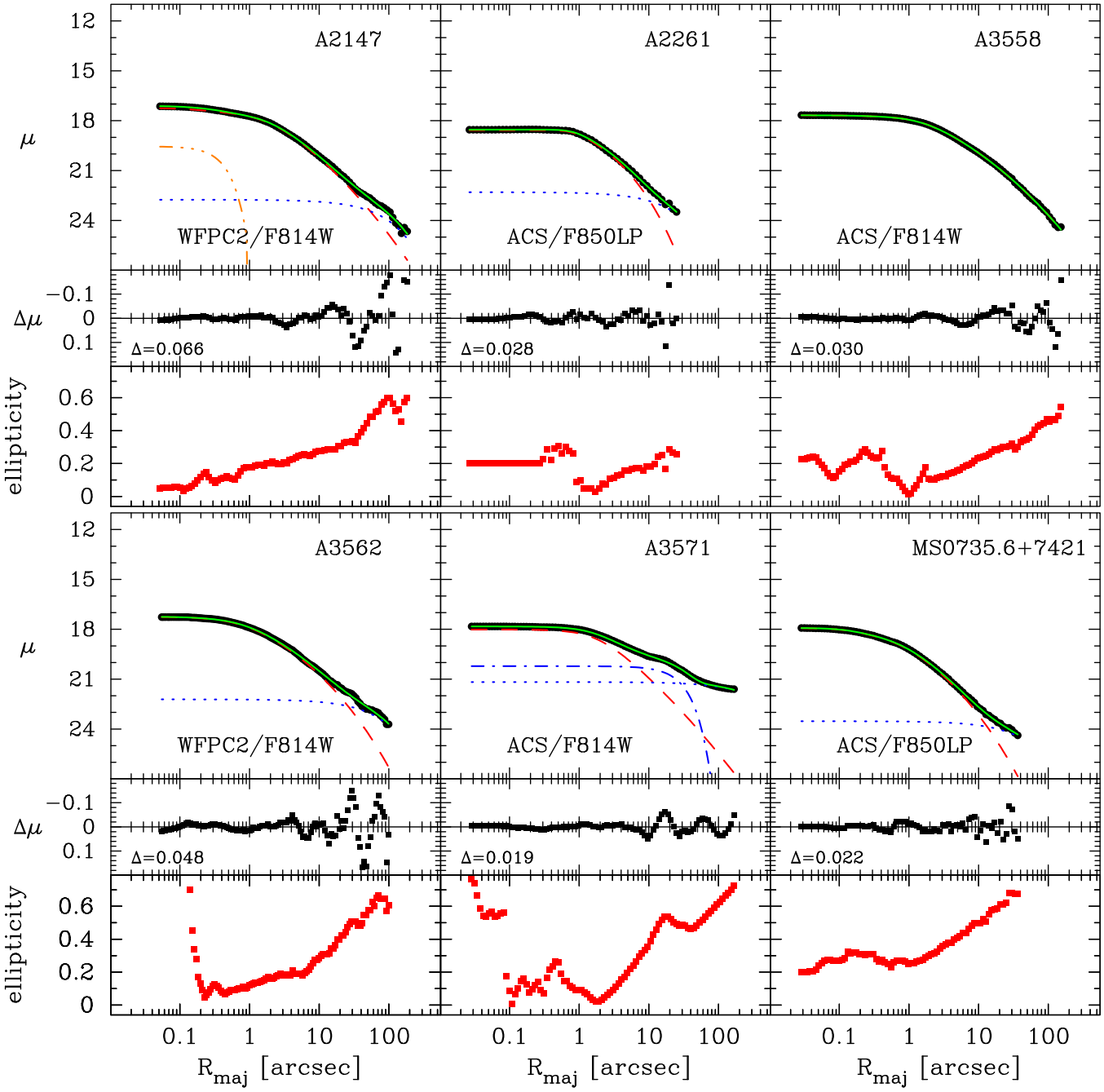

Figure 13. (Continued.)

Appendix B

Spatial distribution of our large-core galaxies and their nearest neighbors (Figure 14).

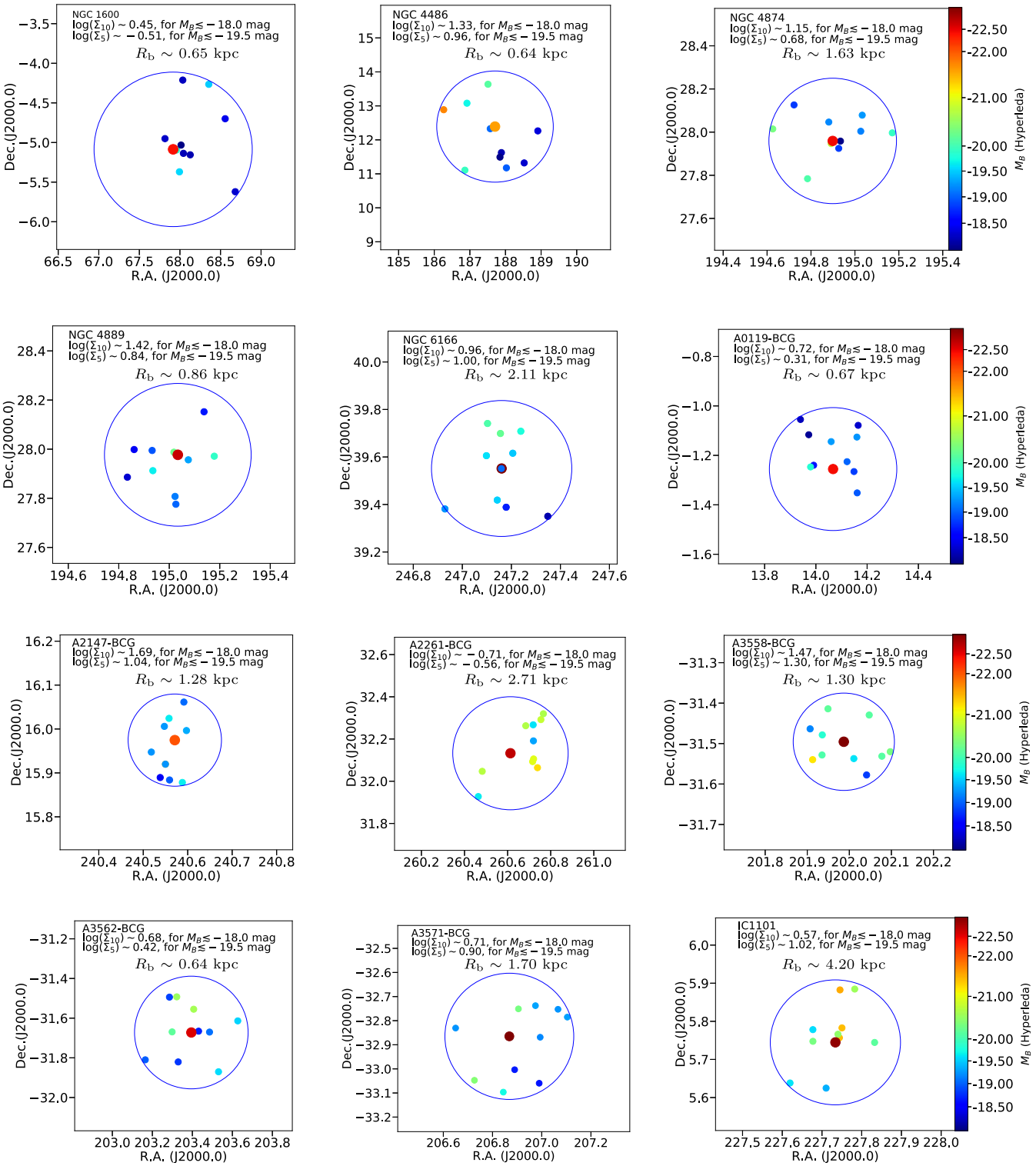

Figure 14. Spatial distribution of our large-core galaxies (big filled circles) and their 10 nearest neighbors with $M_B \lesssim -18.0$ mag and $|V_{\rm hel,large\text{-}core} - V_{\rm hel,neighbour}| < 300$ km s^{-1} (small filled circles). The spatial distribution, nearest neighbor identification, and recession velocities ($V_{\rm hel}$) are based on NED, while the B-band absolute galaxy magnitudes are from Hyperleda. We excluded the sample galaxy 4C +74.13 with no robust data for its nearest neighbors in NED. The blue solid circles, centered on the large-core galaxies, enclose the 10 nearest neighbors. $\Sigma_{10} = N_{\rm gal}/(\pi R_{10}^2)$ and $\Sigma_5 = N_{\rm gal}/(\pi R_5^2)$ are the surface density measurements in Mpc^{-2}, where the radius R_5 (R_{10}), centered on the large-core galaxies, encloses the 5 (10) nearest neighbors with $M_B \lesssim -19.5$ mag ($M_B \lesssim -18.0$ mag), see Cappellari et al. (2011, their Section 3.1). The caveat here is that galaxies with $M_B \gtrsim -19.5$ mag may be too faint to be detected at the distances of 4C +74.13 ($D \sim 925$ Mpc), A2261-BCG ($D \sim 959$ Mpc), and IC 1101 ($D \sim 363$ Mpc). Therefore, we caution that for A2261-BCG and IC 1101, the Σ_{10} values are likely biased toward low values compared to other large-core galaxies shown here with $D \lesssim 213$ Mpc.

ORCID iDs

Bililign T. Dullo https://orcid.org/0000-0002-4140-0110

References

Alamo-Martínez, K. A., & Blakeslee, J. P. 2017, ApJ, 849, 6
Baldry, I. K., Driver, S. P., Loveday, J., et al. 2012, MNRAS, 421, 621
Barnes, J. E. 1988, ApJ, 331, 699
Barrows, R. S., Stern, D., Madsen, K., et al. 2012, ApJ, 744, 7
Begelman, M. C., Blandford, R. D., & Rees, M. J. 1980, Natur, 287, 307
Bell, E. F., Phleps, S., Somerville, R. S., et al. 2006, ApJ, 652, 270
Bender, R., Kormendy, J., Cornell, M. E., & Fisher, D. B. 2015, ApJ, 807, 56
Benson, A. J., Bower, R. G., Frenk, C. S., et al. 2003, ApJ, 599, 38
Bernardi, M., Hyde, J. B., Sheth, R. K., Miller, C. J., & Nichol, R. C. 2007, AJ, 133, 1741
Bernardi, M., Roche, N., Shankar, F., & Sheth, R. K. 2011, MNRAS, 412, L6
Bertin, E., & Arnouts, S. 1996, A&AS, 117, 393
Bianchi, S., Chiaberge, M., Piconcelli, E., Guainazzi, M., & Matt, G. 2008, MNRAS, 386, 105
Binney, J., & Mamon, G. A. 1982, MNRAS, 200, 361
Bluck, A. F. L., Conselice, C. J., Buitrago, F., et al. 2012, ApJ, 747, 34
Bonfini, P., Dullo, B. T., & Graham, A. W. 2015, ApJ, 807, 136
Bonfini, P., & Graham, A. W. 2016, ApJ, 829, 81
Boylan-Kolchin, M., Ma, C.-P., & Quataert, E. 2004, ApJL, 613, L37
Boylan-Kolchin, M., Ma, C.-P., & Quataert, E. 2006, MNRAS, 369, 1081
Brown, W. R., Cohen, J. G., Geller, M. J., & Kenyon, S. J. 2012, ApJL, 754, L2
Burke, C., Hilton, M., & Collins, C. 2015, MNRAS, 449, 2353
Burke-Spolaor, S. 2011, MNRAS, 410, 2113
Byun, Y.-I., Grillmair, C. J., Faber, S. M., et al. 1996, AJ, 111, 1889
Caon, N., Capaccioli, M., & D'Onofrio, M. 1993, MNRAS, 265, 1013
Cappellari, M., Emsellem, E., Krajnović, D., et al. 2011, MNRAS, 416, 1680
Carollo, C. M., Franx, M., Illingworth, G. D., & Forbes, D. A. 1997, ApJ, 481, 710
Carter, D. 1977, MNRAS, 178, 137
Ciotti, L., Lanzoni, B., & Volonteri, M. 2007, ApJ, 658, 65
Comerford, J. M., Pooley, D., Barrows, R. S., et al. 2015, ApJ, 806, 219
Conselice, C. J. 2007, in IAU Symp. 235, Galaxy Evolution Across the Hubble Time, ed. F. Combes & J. Palouš (Cambridge: Cambridge Univ. Press), 381
Cooper, A. P., Gao, L., Guo, Q., et al. 2015, MNRAS, 451, 2703
Crane, P., Stiavelli, M., King, I. R., et al. 1993, AJ, 106, 1371
Davies, R. L., Efstathiou, G., Fall, S. M., Illingworth, G., & Schechter, P. L. 1983, ApJ, 266, 41
Davis, B. L., Graham, A. W., & Cameron, E. 2019, ApJ, 873, 85
de la Rosa, I. G., La Barbera, F., Ferreras, I., et al. 2016, MNRAS, 457, 1916
De Lucia, G., & Blaizot, J. 2007, MNRAS, 375, 2
de Ruiter, H. R., Parma, P., Capetti, A., et al. 2005, A&A, 439, 487
de Vaucouleurs, G. 1948, AnAp, 11, 247
de Vaucouleurs, G., de Vaucouleurs, A., Corwin, H. G., Jr., et al. 1991, Third Reference Catalogue of Bright Galaxies. Volume I: Explanations and references. Volume II: Data for galaxies between 0^h and 12^h. Volume III: Data for galaxies between 12^h and 24^h (Berlin: Springer)
di Tullio, G. A. 1979, A&AS, 37, 591
Donzelli, C. J., Muriel, H., & Madrid, J. P. 2011, ApJS, 195, 15
Dressler, A. 1981, ApJ, 243, 26
Dubinski, J. 1998, ApJ, 502, 141
Dullo, B. T., Chamorro-Cazorla, M., Gil de Paz, A., et al. 2019, ApJ, 871, 9
Dullo, B. T., & Graham, A. W. 2012, ApJ, 755, 163
Dullo, B. T., & Graham, A. W. 2013, ApJ, 768, 36
Dullo, B. T., & Graham, A. W. 2014, MNRAS, 444, 2700
Dullo, B. T., & Graham, A. W. 2015, ApJ, 798, 55
Dullo, B. T., Graham, A. W., & Knapen, J. H. 2017, MNRAS, 471, 2321
Dullo, B. T., Knapen, J. H., Williams, D. R. A., et al. 2018, MNRAS, 475, 4670
Dullo, B. T., Martínez-Lombilla, C., & Knapen, J. H. 2016, MNRAS, 462, 3800
Duncan, K., Conselice, C. J., Mundy, C., et al. 2019, ApJ, 876, 110
Ebisuzaki, T., Makino, J., & Okumura, S. K. 1991, Natur, 354, 212
Edwards, L. O. V., & Patton, D. R. 2012, MNRAS, 425, 287
Efstathiou, G., Ellis, R. S., & Peterson, B. A. 1988, MNRAS, 232, 431
Faber, S. M., & Jackson, R. E. 1976, ApJ, 204, 668
Faber, S. M., Tremaine, S., Ajhar, E. A., et al. 1997, AJ, 114, 1771
Feigelson, E. D., & Babu, G. J. 1992, ApJ, 397, 55
Ferrarese, L., Côté, P., Jordán, A., et al. 2006, ApJS, 164, 334
Ferrarese, L., & Ford, H. 2005, SSRv, 116, 523
Ferrarese, L., & Merritt, D. 2000, ApJL, 539, L9
Ferrarese, L., van den Bosch, F. C., Ford, H. C., Jaffe, W., & O'Connell, R. W. 1994, AJ, 108, 1598
Fukugita, M., Shimasaku, K., & Ichikawa, T. 1995, PASP, 107, 945
Gebhardt, K., Adams, J., Richstone, D., et al. 2011, ApJ, 729, 119
Gebhardt, K., Bender, R., Bower, G., et al. 2000, ApJL, 539, L13
Gebhardt, K., Richstone, D., Ajhar, E. A., et al. 1996, AJ, 112, 105
Gebhardt, K., Richstone, D., Tremaine, S., et al. 2003, ApJ, 583, 92
Gonzalez, A. H., Zabludoff, A. I., & Zaritsky, D. 2003, Ap&SS, 285, 67
Gonzalez, A. H., Zabludoff, A. I., & Zaritsky, D. 2005, ApJ, 618, 195
Goulding, A. D., Pardo, K., Greene, J. E., et al. 2019, ApJL, 879, L21
Graham, A. W. 2004, ApJL, 613, L33
Graham, A. W. 2013, in Planets, Stars and Stellar Systems Vol. 6, ed. T. D. Oswalt & W. C. Keel (Dordrecht: Springer), 91
Graham, A. W. 2016, in Galactic Bulges, ed. E. Laurikainen, R. Peletier, & D. Gadotti, 263
Graham, A. W., & Driver, S. P. 2007, ApJ, 655, 77
Graham, A. W., Dullo, B. T., & Savorgnan, G. A. D. 2015, ApJ, 804, 32
Graham, A. W., Erwin, P., Trujillo, I., & Asensio Ramos, A. 2003, AJ, 125, 2951
Graham, A. W., & Scott, N. 2013, ApJ, 764, 151
Gualandris, A., & Merritt, D. 2008, ApJ, 678, 780
Held, E. V., de Zeeuw, T., Mould, J., & Picard, A. 1992, AJ, 103, 851
Hills, J. G. 1988, Natur, 331, 687
Hilz, M., Naab, T., Ostriker, J. P., et al. 2012, MNRAS, 425, 3119
Hilz, M., Naab, T., & Ostriker, J. P. 2013, MNRAS, 429, 2924
Hlavacek-Larrondo, J., Fabian, A. C., Edge, A. C., & Hogan, M. T. 2012, MNRAS, 424, 224
Hopkins, P. F., & Hernquist, L. 2010, MNRAS, 407, 447
Hopkins, P. F., Lauer, T. R., Cox, T. J., Hernquist, L., & Kormendy, J. 2009, ApJS, 181, 486
Hyde, J. B., Bernardi, M., Sheth, R. K., & Nichol, R. C. 2008, MNRAS, 391, 1559
Jaffe, W., Ford, H. C., O'Connell, R. W., van den Bosch, F. C., & Ferrarese, L. 1994, AJ, 108, 1567
Jedrzejewski, R. I. 1987, MNRAS, 226, 747
Jiménez-Teja, Y., & Dupke, R. 2016, ApJ, 820, 49
Johansson, P. H., Naab, T., & Ostriker, J. P. 2012, ApJ, 754, 115
Kauffmann, G., White, S. D. M., & Guiderdoni, B. 1993, MNRAS, 264, 201
Khosroshahi, H. G., Ponman, T. J., & Jones, L. R. 2006, MNRAS, 372, L68
King, A., & Nealon, R. 2019, MNRAS, 487, 4827
King, I. R. 1978, ApJ, 222, 1
King, I. R., & Minkowski, R. 1966, ApJ, 143, 1002
Kochanek, C. S., Pahre, M. A., Falco, E. E., et al. 2001, ApJ, 560, 566
Komossa, S., Burwitz, V., Hasinger, G., et al. 2003, ApJL, 582, L15
Kormendy, J. 1999, in ASP Conf. Ser. 182, Galaxy Dynamics—A Rutgers Symposium, ed. D. R. Merritt, M. Valluri, & J. A. Sellwood (San Francisco, CA: ASP)
Kormendy, J., & Bender, R. 2013, ApJL, 769, L5
Kormendy, J., Dressler, A., Byun, Y. I., et al. 1994, in ESO Conf. Proc. 49, Workshop on Dwarf Galaxies, ed. G. Meylan & P. Prugniel (Garching: ESO), 147
Kormendy, J., Fisher, D. B., Cornell, M. E., & Bender, R. 2009, ApJS, 182, 216
Kormendy, J., & Ho, L. C. 2013, ARA&A, 51, 511
Kormendy, J., & Richstone, D. 1995, ARA&A, 33, 581
Krajnović, D., Emsellem, E., den Brok, M., et al. 2018, MNRAS, 477, 5327
Kulkarni, G., & Loeb, A. 2012, MNRAS, 422, 1306
Laine, S., van der Marel, R. P., Lauer, T. R., et al. 2003, AJ, 125, 478
Laporte, C. F. P., White, S. D. M., Naab, T., & Gao, L. 2013, MNRAS, 435, 901
Lauer, T. R. 1985, ApJS, 57, 473
Lauer, T. R., Ajhar, E. A., Byun, Y.-I., et al. 1995, AJ, 110, 2622
Lauer, T. R., Faber, S. M., Richstone, D., et al. 2007a, ApJ, 662, 808
Lauer, T. R., Gebhardt, K., Faber, S. M., et al. 2007b, ApJ, 664, 226
Li, Z.-Y., Ho, L. C., Barth, A. J., & Peng, C. Y. 2011, ApJS, 197, 22
Lidman, C., Iacobuta, G., Bauer, A. E., et al. 2013, MNRAS, 433, 825
Liu, F. S., Mao, S., Deng, Z. G., Xia, X. Y., & Wen, Z. L. 2009, MNRAS, 396, 2003
Liu, X., Hou, M., Li, Z., et al. 2019, arXiv:1907.10639
López-Cruz, O., Añorve, C., Birkinshaw, M., et al. 2014, ApJL, 795, L31
Lugger, P. M. 1984, ApJ, 286, 106
Madrid, J. P., & Donzelli, C. J. 2016, ApJ, 819, 50
Magorrian, J., Tremaine, S., Richstone, D., et al. 1998, AJ, 115, 2285
Malumuth, E. M., & Kirshner, R. P. 1981, ApJ, 251, 508

Man, A. W. S., Zirm, A. W., & Toft, S. 2016, ApJ, 830, 89
Marconi, A., & Hunt, L. K. 2003, ApJL, 589, L21
Matković, A., & Guzmán, R. 2005, MNRAS, 362, 289
McConnell, N. J., & Ma, C.-P. 2013, ApJ, 764, 184
McConnell, N. J., Ma, C.-P., Gebhardt, K., et al. 2011, Natur, 480, 215
McConnell, N. J., Ma, C.-P., Murphy, J. D., et al. 2012, ApJ, 756, 179
McNamara, B. R., Kazemzadeh, F., Rafferty, D. A., et al. 2009, ApJ, 698, 594
Mehrgan, K., Thomas, J., Saglia, R., et al. 2019, arXiv:1907.10608
Merritt, D. 2006, ApJ, 648, 976
Merritt, D., Milosavljević, M., Favata, M., Hughes, S. A., & Holz, D. E. 2004, ApJL, 607, L9
Mezcua, M., Hlavacek-Larrondo, J., Lucey, J. R., et al. 2018, MNRAS, 474, 1342
Milosavljević, M., & Merritt, D. 2001, ApJ, 563, 34
Milosavljević, M., Merritt, D., Rest, A., & van den Bosch, F. C. 2002, MNRAS, 331, L51
Montes, M., & Trujillo, I. 2018, MNRAS, 474, 917
Morgan, W. W., & Lesh, J. R. 1965, ApJ, 142, 1364
Mundy, C. J., Conselice, C. J., Duncan, K. J., et al. 2017, MNRAS, 470, 3507
Naab, T., Johansson, P. H., & Ostriker, J. P. 2009, ApJL, 699, L178
Nipoti, C., Londrillo, P., & Ciotti, L. 2003, MNRAS, 342, 501
Oegerle, W. R., & Hoessel, J. G. 1991, ApJ, 375, 15
Oemler, A., Jr. 1974, ApJ, 194, 1
O'Leary, R. M., & Loeb, A. 2008, MNRAS, 383, 86
Oser, L., Naab, T., Ostriker, J. P., & Johansson, P. H. 2012, ApJ, 744, 63
Oser, L., Ostriker, J. P., Naab, T., Johansson, P. H., & Burkert, A. 2010, ApJ, 725, 2312
Paturel, G., Petit, C., Prugniel, P., et al. 2003, A&A, 412, 45
Phipps, F., Bogdan, A., Lovisari, L., et al. 2019, ApJ, 875, 141
Pierini, D., Zibetti, S., Braglia, F., et al. 2008, A&A, 483, 727
Pillepich, A., Nelson, D., Hernquist, L., et al. 2018, MNRAS, 475, 648
Porter, A. C., Schneider, D. P., & Hoessel, J. G. 1991, AJ, 101, 1561
Postman, M., & Lauer, T. R. 1995, ApJ, 440, 28
Postman, M., Lauer, T. R., Donahue, M., et al. 2012, ApJ, 756, 159
Quinlan, G. D., & Hernquist, L. 1997, NewA, 2, 533
Rantala, A., Johansson, P. H., Naab, T., Thomas, J., & Frigo, M. 2018, ApJ, 864, 113
Ravindranath, S., Ho, L. C., Peng, C. Y., Filippenko, A. V., & Sargent, W. L. W. 2001, AJ, 122, 653
Redmount, I. H., & Rees, M. J. 1989, ComAp, 14, 165
Rest, A., van den Bosch, F. C., Jaffe, W., et al. 2001, AJ, 121, 2431
Richings, A. J., Uttley, P., & Körding, E. 2011, MNRAS, 415, 2158
Richstone, D., Ajhar, E. A., Bender, R., et al. 1998, Natur, 395, A14
Robitaille, T., & Bressert, E. 2012, APLpy v2.0.2: Astronomical Plotting Library in Python, Astrophysics Source Code Library, ascl:1208.017
Rodriguez, C., Taylor, G. B., Zavala, R. T., et al. 2006, ApJ, 646, 49
Rodriguez-Gomez, V., Pillepich, A., Sales, L. V., et al. 2016, MNRAS, 458, 2371
Rusli, S. P., Erwin, P., Saglia, R. P., et al. 2013, AJ, 146, 160
Sahu, N., Graham, A. W., & Davis, B. L. 2019, arXiv:1908.06838
Savorgnan, G. A. D., & Graham, A. W. 2015, MNRAS, 446, 2330
Schlafly, E. F., & Finkbeiner, D. P. 2011, ApJ, 737, 103
Schombert, J. M. 1986, ApJS, 60, 603
Schweizer, F. 1982, ApJ, 252, 455
Seigar, M. S., Graham, A. W., & Jerjen, H. 2007, MNRAS, 378, 1575
Sérsic, J. L. 1963, BAAA, 6, 41
Sérsic, J. L. 1968, Atlas de Galaxias Australes
Sheth, R. K., Bernardi, M., Schechter, P. L., et al. 2003, ApJ, 594, 225
Thomas, J., Ma, C.-P., McConnell, N. J., et al. 2016, Natur, 532, 340
Thomas, J., Saglia, R. P., Bender, R., Erwin, P., & Fabricius, M. 2014, ApJ, 782, 39
Toomre, A., & Toomre, J. 1972, ApJ, 178, 623
Trujillo, I., Aguerri, J. A. L., Cepa, J., & Gutiérrez, C. M. 2001, MNRAS, 328, 977
Trujillo, I., Erwin, P., Asensio Ramos, A., & Graham, A. W. 2004, AJ, 127, 1917
van den Bosch, F. C., Ferrarese, L., Jaffe, W., Ford, H. C., & O'Connell, R. W. 1994, AJ, 108, 1579
Veale, M., Ma, C.-P., Thomas, J., et al. 2017, MNRAS, 464, 356
Volonteri, M., & Ciotti, L. 2013, ApJ, 768, 29
West, M. J., de Propris, R., Bremer, M. N., & Phillipps, S. 2017, NatAs, 1, 0157
White, S. D. M., & Rees, M. J. 1978, MNRAS, 183, 341
Worthey, G. 1994, ApJS, 95, 107
Wu, X.-B., Wang, F., Fan, X., et al. 2015, Natur, 518, 512
Young, P. J., Westphal, J. A., Kristian, J., Wilson, C. P., & Landauer, F. P. 1978, ApJ, 221, 721
Zibetti, S., White, S. D. M., Schneider, D. P., & Brinkmann, J. 2005, MNRAS, 358, 949
Zolotov, A., Willman, B., Brooks, A. M., et al. 2009, ApJ, 702, 1058